Cancer Immunology, Immunotherapy (2026) 75:145
https://doi.org/10.1007/s00262-026-04387-y

RESEARCH

Promoting APC function of B cells via reprogramming the fatty acid metabolism enhances anticancer immunity in metastatic ovarian cancer

Haoke Zhang[1] · Chunyan Yu[1] · Wei Du[1] · Huiyang Li[2] · Zihe Liu[1] · Xueying Li[1] · Yuhan Yue[3] · Bo Wang[1] · Hongmei Wang[4] · Yuqing Ouyang[1] · Haixia Wu[5] · Xiaofan Feng[1] · Jianchun Yu[6] · Yaru Liu[1] · Boyu Ji[1] · Siyu Cai[1] · Hong Zhang[1] · Weimin Deng[1]

Received: 28 October 2025 / Accepted: 27 March 2026

Abstract

B cells have become one of the important participants in anti-tumor immunity. Compared with DCs and macrophages, B cells have unique advantages in presenting low-abundance antigens to T cells. Fatty acids play a key role in the metabolic adaptation of B cells. Whether the APC function of B cells can be enhanced through reprogramming fatty acid metabolism in the tumor microenvironment (TME) is worthy of study. Ovarian cancer (OvCa) is a gynecological malignant tumor with a high mortality rate. Most patients in the advanced stage often have extensive omental metastasis and ascites formation, which are rich in adipocytes and fatty acids. Given reasons including complex TME, the clinical efficacy of new immunotherapies such as immune checkpoint blockade (ICB) therapy for OvCa is very limited. Therefore, treatment regimens based on new mechanisms are urgently needed to be developed. In this study, we applied the Gene Expression Omnibus (GEO) database, clinical specimens, cell lines, and mouse models to investigate whether reprogramming the fatty acid metabolism in B cells could enhance their APC function and to explore the underlying mechanisms. We also evaluated the therapeutic effects of the combined treatment using APC-enhanced-B cells adoption with low-dose chemotherapy in metastatic OvCa mice. Our research provides new clues forB cells-based anti-tumor immunotherapy.

Keywords B cells · Fatty acid metabolism · Antigen presentation · Anticancer immunity · Ovarian cancer

Introduction

B cells are now recognized as one of the major contributors to anticancer immunity and have strong prognostic significance in various human cancers [1]. B cells not only directly participate in immune responses by secreting antibodies and

Haoke Zhang, Chunyan Yu, Wei Du, Huiyang Li, Zihe Liu, These authors contributed equally to this work.

✉ Weimin Deng
dengweimin@tmu.edu.cn

[1] Department of Immunology, Tianjin Key Laboratory of Cellular and Molecular Immunology, Key Laboratory of Diseases and Microenvironment of Ministry of Education of China, Tianjin Institute of Immunology, Tianjin Medical University, No.22 Qixiangtai Road, Heping District, Tianjin 300070, China

[2] Department of Gynecology and Obstetrics, Tianjin Key Laboratory of Female Reproductive Health and Eugenics, Tianjin Medical University General Hospital, Tianjin 300052, China

[3] Inner Mongolia Cancer Center, Peking University Cancer Hospital (Inner Mongolia Campus)/Affiliated Cancer Hospital of Inner Mongolia Medical University, Inner Mongolia Autonomous Region, Hohhot 010000, China

[4] School of Basic Medical Sciences, Tianjin Medical University, Tianjin 300070, China

[5] Department of Pathology, Tianjin Central Hospital of Gynecology Obstetrics, Tianjin 300100, China

[6] Central Laboratory, First Teaching Hospital of Tianjin University of Traditional Chinese Medicine, Tianjin 300193, China

Published online: 15 April 2026

producing cytokines to affect tumor growth and treatment responses, but also act as antigen-presenting cells (APCs) by expressing high levels of costimulatory molecules such as CD80 and CD86 and major histocompatibility complex (MHC) molecules, presenting processed antigen products to T cells to activate them and facilitate adaptive immune responses against cancer [2–4]. Moreover, B cells have the unique advantage of presenting low-abundance antigens to T cells more effectively than dendritic cells or macrophages [5]. In the TME, B cells engage in intricate crosstalk not only with T cells but also with other immune cells, such as follicular dendritic cells (FDCs), collectively maintaining a "hot" TME characterized by diverse immune infiltrates and promoting the formation of tertiary lymphoid structures (TLS) [6]. B cells are key components of the lymphoid follicles in TLS, which serve as a predominant niche for APC functional B cells. The abundance of B cells demonstrates a positive correlation with TLS density in tumors [7]. Recent advances research have brought increasing attention to the potential application of B cells' APC function in cancer immunotherapy [4].

Fatty acids (FAs) play a critical role in the metabolic adaptation of B cells [8]. Fatty acid (FA) metabolic genes include uptake genes such as fatty acid binding protein 4 (FABP4) and CD36 (also known as FA translocase) [9], catabolic genes such as hormone-sensitive lipase (HSL), acyl coenzyme A dehydrogenase very long chain (ACADVL), carnitine palmitoyltransferase 1A (CPT1A), and the key transcription factor peroxisome proliferator-activated receptor gamma (PPARγ) [10]. Florian J. Weisel et al. reported that in a normal mouse model immunized with alum, germinal center B cells primarily rely on fatty acid oxidation as their major energy source. These cells take up FAs and generate ATP through mitochondrial and peroxisomal FA oxidation to meet their high metabolic demands [11]. Germinal center B cells with metabolic specificity rely on FA oxidation to meet their high proliferative demands [11]. FAs in the TME not only affect the metabolism of cancer cells but also have a significant impact on immune cells, including B cells [12]. The effects of FA metabolism on B cells, especially their APC function in TME, remain unclear.

Ovarian cancer (OvCa) is a gynecological malignancy with a poor prognosis and high mortality rate [13, 14]. Epithelial ovarian cancer (EOC) is the most common histological type of OvCa, accounting for 90% of OvCa cases. High-grade serous ovarian cancer (HGSOC) is the main subtype of EOC [15]. Due to its insidious onset and rapid progression, most EOC patients have been at advanced stages (FIGO III–IV) when diagnosed, accompanied by extensive peritoneal metastasis and ascites formation [16, 17]. The omentum in the abdominal cavity is rich in adipocytes, forming a unique adipose-rich microenvironment. The standard first-line treatment strategies for EOC are tumor reduction and chemotherapy, including platinum or taxane derivatives. However, 70%–80% of patients relapse within 2–5 years and develop resistance to the treatments [18, 19]. The efficacy of immune checkpoint blockade (ICB) targeting PD-1/PD-L1 varies across tumor types. Due to the complex TME of OvCa, ICB demonstrates limited clinical benefits [19], making chemotherapy remain the first-line standard of OvCa treatment [20]. Although the impact of TME on T cell metabolic adaptation has been extensively studied [21], research on how TME influences that of B cells remains limited. The effects and mechanisms of TME on B cells' APC function, as well as therapeutic strategies targeting B cells metabolism, urgently require further investigation and development.

In this study, we applied Gene Expression Omnibus (GEO) databases, clinical specimens, EOC cell lines, and metastatic OvCa mouse models to investigate whether reprogramming the FA metabolism of B cells could enhance their APC functions and explore the mechanisms. Furthermore, we evaluated a novel immunotherapy approach in metastatic OvCa mouse models, combining the adoptive transfer of APC function-enhanced B cells with low-dose chemotherapy (LDC), providing new therapeutic insights for B cells-based cancer immunotherapy.

Materials and methods

Animals

All C57BL/6 mice (17–18 g, 8 w, female) were purchased from Beijing Spafu Biotechnology Co., LTD. Mice were housed in specific pathogen-free (SPF) conditions under a 12h light/dark cycle (lights on at 7:00 AM) at 23 ± 3 °C and $50 \pm 10\%$ humidity. Each cage contained ≤ 5 mice with corn cob bedding and nesting materials for enrichment. Mice had free access to standard rodent chow and sterile water. All animal experiments were performed accordance to guidelines approved by the animal ethics committee of Tianjin Medical University.

Cell lines and cell culture

The mouse ovarian epithelial papillary serous adenocarcinoma cell line ID8 (C57BL/6 background) was obtained from Professor Luyuan Li (Nankai University, Tianjin, China). ID8 cells were cultured in DMEM medium (KGI Biotechnology Co., LTD.) supplemented with 80 U/mL penicillin, 80 µg/mL streptomycin (PS), and 10% (v/v) fetal bovine serum (FBS, Gibco). B cells were cultured in RPMI 1640 medium (KGI Biotechnology Co., LTD.) supplemented with 80 U/mL penicillin and 80 µg/mL streptomycin (PS) and 10% (v/v) FBS. ID8 cells were routinely tested for

mycoplasma contamination and maintained at low passage numbers (< 10).

Immunohistochemical (IHC) staining

Tumor tissue samples from HGSOC patients were collected at Tianjin Central Obstetrics and Gynecology Hospital, and IHC staining was performed according to the previously described method [22]. In short, the samples were incubated overnight at 4 °C with primary antibodies (Abs) against CD3, CD19, CD21, CD80, and CD86 (see Table S3), then secondary Abs were added, and diaminobenzidine was used for detection. Finally, the nucleus was re-stained with hematoxylin, and the images were collected under an optical microscope (ZEISS) for analysis. The cells in three independent regions, adjacent to or distant from adipose tissue, in each sample were counted for analysis.

Identification of lymphoid aggregates in ascites of OvCa mice

The ascites or peritoneal lavage fluid from OvCa mice was gently transferred into a petri dish using a syringe and incubated for 2h to allow cancer cells adhesion, and the suspended cells were then carefully collected into a tube and allowed to settle at room temperature for 2h. Then, 20 µL of cell precipitation was carefully transferred onto a glass slide using a 200 µL pipette tip and gently released with the tip to make cell smears. Frozen sections were also prepared by embedding the cell precipitations. $CD3^+$T cells, $CD19^+$B cells, and $CD21^+$FDC were detected by immunofluorescence staining and observed under a confocal microscope. 5 fields in each sample were randomly selected for cell counting. The information on primary Abs is listed in Table S3. Secondary Abs included Alexa Fluor™ 647 (Goat anti-rat, 1:1000, Invitrogen; Cat# A-21247), Alexa Fluor™ 594 (Goat Anti-Rabbit, 1:1000, Abcam; Cat# ab150080). Considering the integrity of lymphoid aggregates may be affected by manipulations, all pipette tips were snipped to ensure the lymphoid aggregates were not damaged, and each operation was carefully and gently performed. Our laboratory defined the cell aggregates of "FDC (≥ 1) + B cells (≥ 2) + T cells (≥ 1)" observed under a confocal microscope (the spatial positions of the cells are FDC-B-T) as one typical lymphoid aggregates.

Magnetic bead sorting (MACS)

The splenic single-cell suspension was prepared, and the peritoneal lavage fluid or ascites was collected from metastatic OvCa mice. The red blood cells were removed using red blood cell lysate. The ascitic cells were resuspended and cultured at 37 °C for 2h to allow cancer cell adhesion to the dish, and then the suspended lymphocytes were collected. ImunoSep mouse $CD19^+$B cell positive selection kit (Precision BioMedicals; Cat# 721,920) was used to obtain $CD19^+$B cells. ImunoSep mouse $CD3^+$T cell positive selection kit (Precision BioMedicals; Cat# 720,305) was used to obtain $CD3^+$T cells.

In vitro *treatment of B cells*

Human $CD19^+$B cells, mouse splenic $CD19^+$B cells (1×10^6/mL) or mouse ascitic $CD19^+$B cells were treated with 150 µM oleic acid (OA) or palmitic acid (PA) for 24h. For in vitro pre-activation, mouse ascitic $CD19^+$B cells were pretreated with 10 µg/mL CD40L and 10 ng/mL IL-4 for 24h [23]. In the mechanistic study, mouse ascitic $CD19^+$B cells (1×10^6/ml) were pretreated with fatty acid binding protein 4 gene (FABP4) inhibitor (BMS309403, MedChemExpress; Cat# HY-101903; 50 µM), PPARγ antagonist (GW9662, MedChemExpress; Cat# HY-16578; 25 µM), and PPARγ agonist (Troglitazone, Trog, MedChemExpress; Cat# HY-50935; 10 µM) for 2h, respectively. Then the cells were washed with PBS twice, inoculated on a 12-well plate, and treated with 150 µM OA for 24h. B cells were then collected and analyzed by flow cytometry.

Flow cytometry

The prepared single-cell suspension (1×10^6/ml) of $CD19^+$B cells or ascitic cells was resuspended in Zombie NIR live/dead stain (Biolegend; Cat# 423,105) and incubated for 15 to 30 min at room temperature. Cells were washed twice, then resuspended in 100 µl FACS buffer (2% FBS, 1 mM EDTA in PBS), and incubated with fluorescence-labeled Abs listed in Table S3. For intracellular detection of IFN-γ, GZMB, IL-2, and IL-10, cells were first stimulated with a cell activation reagent (BioLegend; Cat# 423,303) for 6h and then incubated with the corresponding antibodies. Surface antigens (e.g., CD45, CD3, CD19, CD8) were stained, followed by fixation with 4% paraformaldehyde. Cells were then permeabilized using Intracellular Staining Perm Wash Buffer (10×) (BioLegend; Cat# 421,002) diluted to 1× according to the manufacturer's instructions. C16-BODIPY was used to detect intracellular FA content in cells. C11-BODIPY was used to detect lipid peroxide in cells. The cells were detected using Flow Cytometry (BD Bioscience), and the data were analyzed using FlowJo V10 software.

Transfection of small interfering RNA (siRNA)

The siRNA targeting mouse FABP4 (siFABP4) and non-silencing negative control siRNA (siNC) were synthesized by Ribobio (Guangzhou, China). The sequences of two siFABP4 oligonucleotides are GGGCTTTGCCACAAG

GAAA and GGTGGAATGTGTTATGAAA. According to the manufacturer's instructions, mouse ascitic $CD19^+$B cells were collected and resuspended in serum-free buffer. siRNA oligonucleotides were transfected into the cells using the ProteanFect Max Mouse Primary Immune Cell Transfection Kit (Nanoportal Biotech; Cat# PT03) with a final siRNA concentration 200 pmol/100 μL. The transfection complexes were incubated with cells for 30 min at 37 °C. Cells were harvested 24h after transfection for subsequent analyses.

RNA sequencing (RNA-seq)

Ascitic $CD19^+$B cells were seeded in a 75 cm^2 flask (1×10^6) and cocultured with OA for 24h. Suspended $CD19^+$B cells were then isolated using a mouse lymphocyte separator (Tianjin Haoyang Huake Biotechnology Co., Ltd.; Cat# LTS1092). Cells were lysed with 1 mL of TRIzol reagent (Tiangen Biotech, Co., Ltd.; Cat# DP424), and the samples were sent to Tiangen Biotech, Co., Ltd. for RNA sequencing and analysis. According to the manufacturer's instructions, RNA with Poly-A structure was enriched from total RNA using the TIANSeq mRNA capture kit (TIANGEN Biotech). Then, the captured RNA was used as the starting sample for library construction with the TIANSeq rapid RNA library construction kit (Illumina Platform, TIANGEN Biotech). The RNA library was then analyzed with the Agilent 2100 Bioanalyzer. After the library test was qualified, PE150 sequencing was performed using the Illumina Platform to obtain 150-bp paired-end sequencing reads. The data can be found in Table S1.

Reverse transcription-polymerase chain reaction (RT-PCR)

Total RNA was extracted from 1×10^6 mouse ascitic $CD19^+$B cells using TRIzol. The TransScript® one-step gDNA Removal and cDNA Synthesis SuperMix (Beijing Quanshi Jin Biotechnology Co., LTD.; Cat# AT311-03) was used to remove genomic DNA and synthesize cDNA, followed by RT-PCR using primers (see Table S2). PCR products were analyzed by agarose gel electrophoresis. β-Actin was used as a reference to calculate the relative mRNA levels.

Western blot (WB) analysis

RIPA lysate (Jiangsu Kaiji Biotechnology Co., LTD.; Cat# KGB5204) was used to lyse the harvested cells. Protease inhibitor (Jiangsu Kaiji Biotechnology Co., LTD.; KGB5101-100) was used to inhibit the activities of phosphatase and protease. According to molecular weights, the proteins were separated on an SDS-PAGE gel and then transferred to a polyvinylidene fluoride (PVDF) membrane, which was incubated with the primary Abs (listed in Table S3) overnight at 4 °C, and then the secondary Abs were added for incubation. The protein bands were scanned using the Odyssey®CLx scanner. The strip density was measured using Odyssey 3.0 software.

A-CoA and ATP levels detected by ELISA

Mouse $CD19^+$B cells were homogenized in cold PBS and centrifuged at 12,000 × g at 4 °C for 10 min to collect the supernatant. The levels of A-CoA and ATP were quantified using a mouse A-CoA ELISA Kit (LunChangShuoBiotech; Cat# ED-21683) and ATP ELISA Kit (LunChangShuoBiotech; Cat# ED-24959). The absorbance was determined at 450 nm (OD450) using a microplate reader (BioTek Instruments, Inc.). Standard curves of mouse A-CoA and ATP were generated to quantify the concentration of A-CoA and ATP.

FAO rate measurement

Mouse $CD19^+$B cells were homogenized in cold PBS and centrifuged at 12,000 × g at 4 °C for 10 min to collect the supernatant. FAO rate was evaluated with a colorimetric assay kit (Elabscience; Cat# E-BC-K784-M) according to the provider's instruction. After standardizing the protein concentration (BCA Protein Assay Kit, KeyGEN; Cat# KGB2101-250), the absorbance at 450 nm was measured. The amount of enzyme in 1 g protein/min that hydrolyzes the substrate to produce NADH at 37 ℃ was defined as 1 unit by the following formula: FAO ability (U/gprot) = (ΔA450-b)/a ÷ T × 1, 000/Cpr (ΔA450: OD sample–OD control. T: reaction time, 30 min. Cpr: concentration of protein in sample).

Cancer cell-killing experiment

The cultured ID8 cells were harvested to prepare antigenic peptides by water bath at 43 °C for 30 min and frozen in liquid nitrogen for 20 min (repeated three times). After centrifugation at 10,000 rpm for 30 min at 4 °C, the supernatant was filtered into a 1.5 mL tube and stored in the refrigerator at −80 °C for future use to pulse B cells. 2×10^5/mL antigen-pulsed B cells and 2×10^5/mL T cells per well were cocultured in a 12-well plate for 6h. Then, 2×10^5/mL ID8-luc cells were directly added and cocultured for 48h. The supernatant was collected for the detection of IFN-γ, Granzyme B (GZMB), and TNF-α using ElaBoXTMMouse IFN-γ ELISA Kit (Solebol; Cat# SEKM-0031), ElaBoXTMMouse Granzyme B ELISA Kit (Solebol; Cat# SEKM-0088), and ElaBoXTMMouse TNF-α ELISA Kit (Solebol; Cat# SEKM-0034) by enzyme-linked immunosorbent assay (ELISA). The absorbance at 450 nm was measured using a

microplate reader (BioTek Instruments, Inc.). The cells at the bottom of the wells were washed twice with PBS. Then, the cell lysis buffer (Luciferase Assay System with Reporter Lysis Buffer, Promega) was used to lyse ID8-luc cells, and the luminescence was detected by the Luminescence Detector (Promega; 2031–000).

In vivo tracing experiment of B cells

1×10^6/mL mouse ascitic $CD19^+$B cells were stained with CM-DiI staining solution (Invitrogen; Cat# C7000, 2 μg/mL), incubated at 37 °C for 5 min and then at 4 °C for 15 min. The CM-DiI-labeled cells were injected intraperitoneally or intravenously into 1 w tumor-bearing recipient mice (1×10^6 cells/100 μL/mouse). The mice were killed, and the organs and tissues were collected. Anticoagulant peripheral blood, ascites, and bone marrow were collected to make smears and fixed with 4% paraformaldehyde. Spleen and inguinal-draining lymph nodes were collected to prepare frozen sections. Nuclei were stained by DAPI (Beyotime), and the smears or frozen sections were observed and imaged under a fluorescence microscope (Leica-DMi8) for analysis.

Chromatin immunoprecipitation

The B cells were fixed in 1% formaldehyde, lysed, and sonicated to shear chromatin into fragments of approximately 200–500 bp. Chromatin from the resulting cell lysates was immunoprecipitated with either an anti-mouse H3K27ac/PPARγ antibody or a normal IgG control (listed in Table S3). The antibody-chromatin complexes were enriched using protein G-agarose beads, after which the DNA was purified. Quantitative PCR (qPCR) was performed using specific primers targeting the promoter regions of PPARγ, CD80, CD86, and CD83 genes (see Table S2). A 10% aliquot of the lysate before immunoprecipitation was used as an input control. The data were normalized to the input DNA and presented as fold enrichment over the IgG control.

B cell adoptive transfer and chemotherapy treatment

ID8-luc cells (3×10^6 cells/200 μL/mouse) were intraperitoneally injected into C57BL/6 mice to establish a metastatic mouse OvCa model. Then, the mice were randomly divided into five groups (n = 3 each) and received intraperitoneal injections as follows: control group (PBS, 200 μL/mouse), group of OA-treated B cells (B_{OA}, 1×10^6/200 μL/mouse, administrated every 3 days [24] and started on the 8th day after tumor-bearing), low-dose cisplatin (L-DDP) group (Qilu Pharmaceutical Co., LTD.; 1 mg/kg [25], administrated once a week and started 1 day after BOA administration), combined group (L-DDP and BOA), and high-dose chemotherapy (H-DDP, 2 mg/kg, administrated same as L-DDP). Bioluminescence imaging (BLI) was performed once a week to monitor tumor development. On the 28th day after tumor-bearing, the mice were killed. Peritoneal lavage fluid or ascites was collected for the analysis of ascitic T cells of B cells. OCT embedding of immune cells in ascites was performed to prepare frozen sections. A parallel survival experiment was performed (n = 7 in each group). The weight and status of the mice were monitored daily. The survival time point was set when the weight of mice reached the cut-off value of 35 g [26]. All mice were anesthetized with 2% isoflurane for 10 min and then killed by cervical dislocation.

Bioinformatics analysis

For RNA-seq, we incorporated paired RNA-seq data ($CD19^+$B group, n = 1; $CD19^+$B + OA group, n = 1). After quality control, a total of detectable genes were obtained. Subsequently, edgeR v3.40 was used to perform differential analysis on the RNA-seq count matrix. The raw counts were structured into a DGEList object, followed by TMM normalization using calcNormFactors to correct for sequencing depth variations. A fixed dispersion strategy was applied, setting the common dispersion to 0.1. The exactTest (exact negative binomial test in edgeR) was then employed to compare gene expression levels between the two groups, with multiple testing corrected by the Benjamini–Hochberg method. Differentially expressed genes (DEGs) were identified based on the criteria of $|\log2FC| > 1$ and $p < 0.05$. Next, the cpm function was used to transform TMM-normalized counts into log2-CPM values, and genes with no expression variation across all samples were filtered out to reduce noise. PCA analysis (centered and scaled) was performed using prcomp, and sample group information was mapped to the dimensionality reduction results. Finally, GSEA enrichment analysis was conducted using the fgsea package.

Datasets GSE281120, GSE184880, GSE235329, GSE276563, GSE290141, GSE242271, GSE235931, GSE147082 and GSE154600 in the GEO database were analyzed. These nine datasets comprise single-cell RNA sequencing data from 48 patients with HGSOC. Datasets GSE235931, GSE147082 and GSE154600 in the GEO database were analyzed. These three datasets comprise single-cell RNA sequencing data from 13 patients with metastatic OvCa. After performing uniform quality control (QC) and batch effect correction across all datasets, integrated analysis was conducted using Seurat v4.3. Differential expression analysis of B cells was performed using the FindMarkers function to identify differentially expressed genes (criteria: $|\log2FC| > 1$, $p < 0.05$, Wilcoxon rank-sum test). Gene set enrichment analysis (GSEA) was carried out using the fgsea package, while fatty acid (FA) metabolic pathway enrichment was analyzed with the GSVA package. Gene

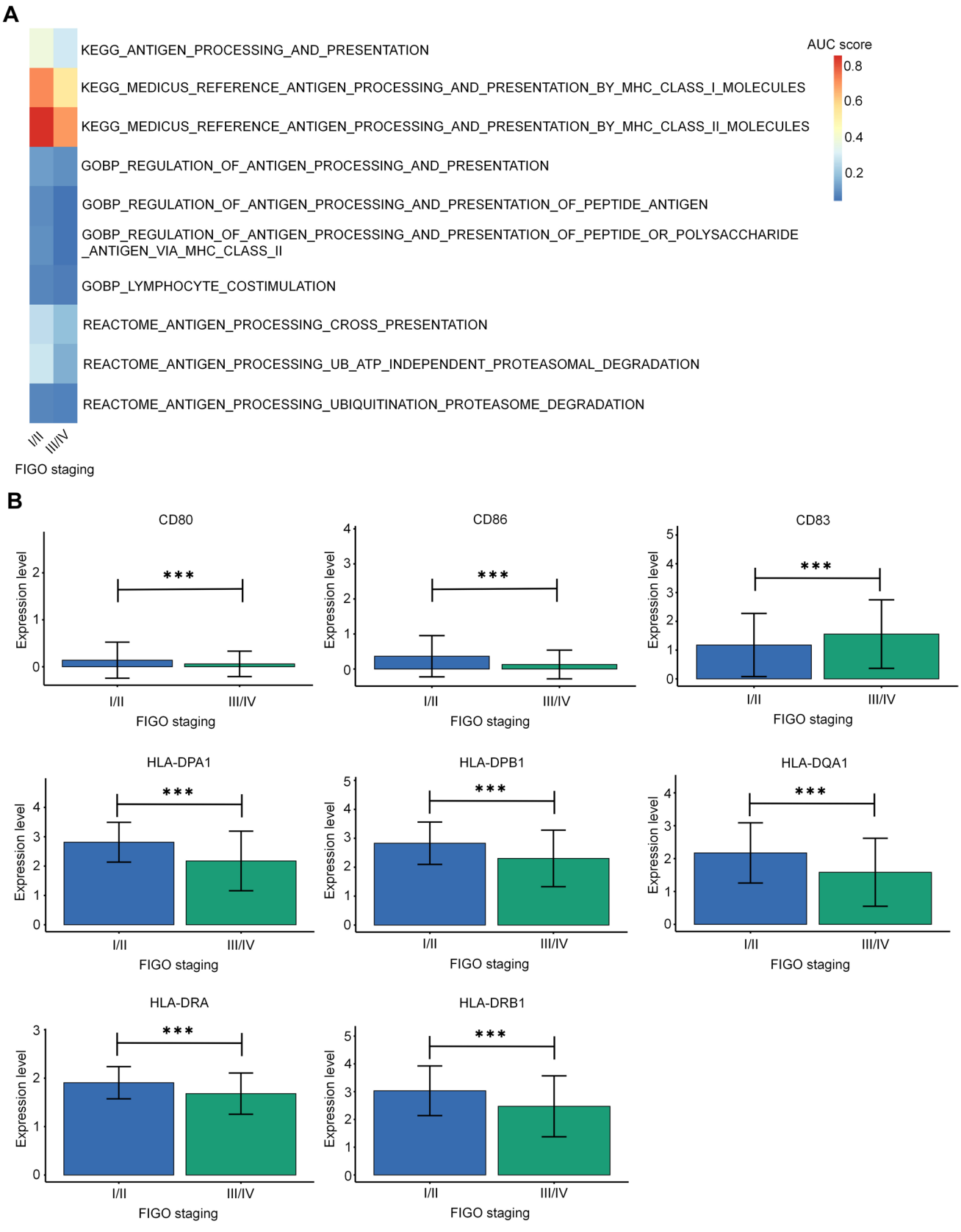
A
KEGG_ANTIGEN_PROCESSING_AND_PRESENTATION
KEGG_MEDICUS_REFERENCE_ANTIGEN_PROCESSING_AND_PRESENTATION_BY_MHC_CLASS_I_MOLECULES
KEGG_MEDICUS_REFERENCE_ANTIGEN_PROCESSING_AND_PRESENTATION_BY_MHC_CLASS_II_MOLECULES
GOBP_REGULATION_OF_ANTIGEN_PROCESSING_AND_PRESENTATION
GOBP_REGULATION_OF_ANTIGEN_PROCESSING_AND_PRESENTATION_OF_PEPTIDE_ANTIGEN
GOBP_REGULATION_OF_ANTIGEN_PROCESSING_AND_PRESENTATION_OF_PEPTIDE_OR_POLYSACCHARIDE_ANTIGEN_VIA_MHC_CLASS_II
GOBP_LYMPHOCYTE_COSTIMULATION
REACTOME_ANTIGEN_PROCESSING_CROSS_PRESENTATION
REACTOME_ANTIGEN_PROCESSING_UB_ATP_INDEPENDENT_PROTEASOMAL_DEGRADATION
REACTOME_ANTIGEN_PROCESSING_UBIQUITINATION_PROTEASOME_DEGRADATION
AUC score
0.8
0.6
0.4
0.2
I/II
III/IV
FIGO staging
B
CD80
CD86
CD83
HLA-DPA1
HLA-DPB1
HLA-DQA1
HLA-DRA
HLA-DRB1
Expression level
***
I/II
III/IV
FIGO staging

◂**Fig. 1** The APC function of B cells decreases with the progression of FIGO staging in patients with OvCa. **A** AUCell pathway enrichment analysis of B cells in patients with HGSOC (GSE281120, GSE184880, GSE235329, GSE276563, GSE290141, GSE242271, GSE235931, GSE147082 and GSE154600 dataset in the GEO database, n = 48). **B** Analysis of differences in the expression of APC function-related genes of B cells in 48 HGSOC patients (dataset GSE281120, GSE184880, GSE235329, GSE276563, GSE290141, GSE242271, GSE235931, GSE147082 and GSE154600). ***$p < 0.001$

Ontology (GO) analysis was performed using the clusterProfiler package.

Protein interaction prediction analysis was conducted through the STRING website (http://www.string-db.org/). Correlation analysis between TLS gene sets [27] or PPARγ and representative B cell genes (CD79A, MZB1, MS4A1, and CD79B), B cell APC functional genes (CD80, CD86, CD83, and MHC II), and fatty acid (FA) metabolism-related genes (FABP4, FATP4, CD36, FASN, HSL, CPT1A, ACADVL, and PPARγ) was performed using the GEPIA2 website (http://gepia2.cancer-pku.cn/#index).

Statistical analysis

Statistical analysis was performed using GraphPad Prism 9.5 software. One-way analysis of variance (ANOVA) was used to compare groups. The statistical difference between the two groups was evaluated using the unpaired T-test. Two-factor ANOVA was used for the analysis of IHC staining and TLS analysis. Survival time was analyzed using a logarithmic rank test (Mantel–Cox test) with data presented as median survival time (MS). Data are presented as mean ± standard deviation (SD). $p < 0.05$ was considered statistically significant.

Results

The APC function of B cells decreases with the progression of FIGO staging in patients with OvCa

To examine the APC function of B cells in patients with OvCa as the disease progresses, we conducted bioinformatics analysis. We integrated and analyzed the single-cell transcriptome data of clinical specimens from 48 HGSOC patients in nine datasets of the GEO database. A total of 217,294 cells were obtained from these samples. Based on the established list of gene markers (Table S4), these cells were clustered and annotated. Cell visualization is achieved through UMAP (Fig. S1 A). B cells were divided into two groups based on the FIGO stage of the source patients, namely FIGO I/II and FIGO III/IV. Subsequently, two groups of B cells were subjected to pathway enrichment analysis through AUCell. The results showed that compared with stage I/II, the APC function-related pathways of B cells in HGSOC patients with stage III/IV decreased significantly (Fig. 1A). Meanwhile, representative genes of APC function-related pathways in B cells in the above two different groups were also compared. The results showed that with tumor progression, the expression of costimulatory molecules (including CD80 and CD86) and MHC class II molecules (such as HLA-DPA1, HLA-DPB1, and HLA-DQA1) decreased significantly (Fig. 1B). This is in line with the trend observed in the results of pathway enrichment analysis. The above results suggest that with the progression of FIGO staging in OvCa patients, the APC function of B cells significantly declines.

The APC function of B cells is closely associated with their FA metabolism in metastatic OvCa

Given the critical role of FAs in B cells metabolic adaptation [12] and the unique lipid-rich microenvironment of metastatic OvCa [16, 17], the first point we consider is whether the APC function of B cells is related to their FA metabolism within TME? To solve this problem, we first utilize bioinformatics data to analyze the relationship between them. We integrated and analyzed the single-cell transcriptome data of 13 patients with metastatic OvCa from three datasets in the GEO database. A total of 66,863 cells were obtained from these samples. According to the established list of marker genes (Table S5), these cells were clustered and annotated (Fig. S1 B). A total of 3563 B cells were extracted for gene expression difference analysis and gene set variation analysis (GSVA). According to the mRNA expression levels of CD80, CD86, and CD83 (the marker for activation of B cells), these B cells were divided into APC function low and APC function high B cell groups (Fig. S1 C-E). Gene set variation analysis (GSVA) was then performed on these two B cell groups. Correlation analysis revealed that compared with the APC function low B cell group, the FA pathway was significantly enriched in the APC function high B cell group (Fig. 2A). These results indicate that in metastatic OvCa, the APC function of B cells is positively correlated with its FA metabolism.

Recently, it has been reported that B cells that perform APC functions are generally located in TLS in solid cancers. Therefore, we also analyzed the correlation between TLS and APC function and FA metabolism of B cells using sequencing data from 426 OvCa patients in the TCGA database. We found that TLS-related gene expression was positively correlated not only with the expression of genes related to the number of B cells, the APC function of B cells but also with that of genes related to FA transport, lipolysis, and FA metabolism of B cells (Fig. S2 A). Moreover, to

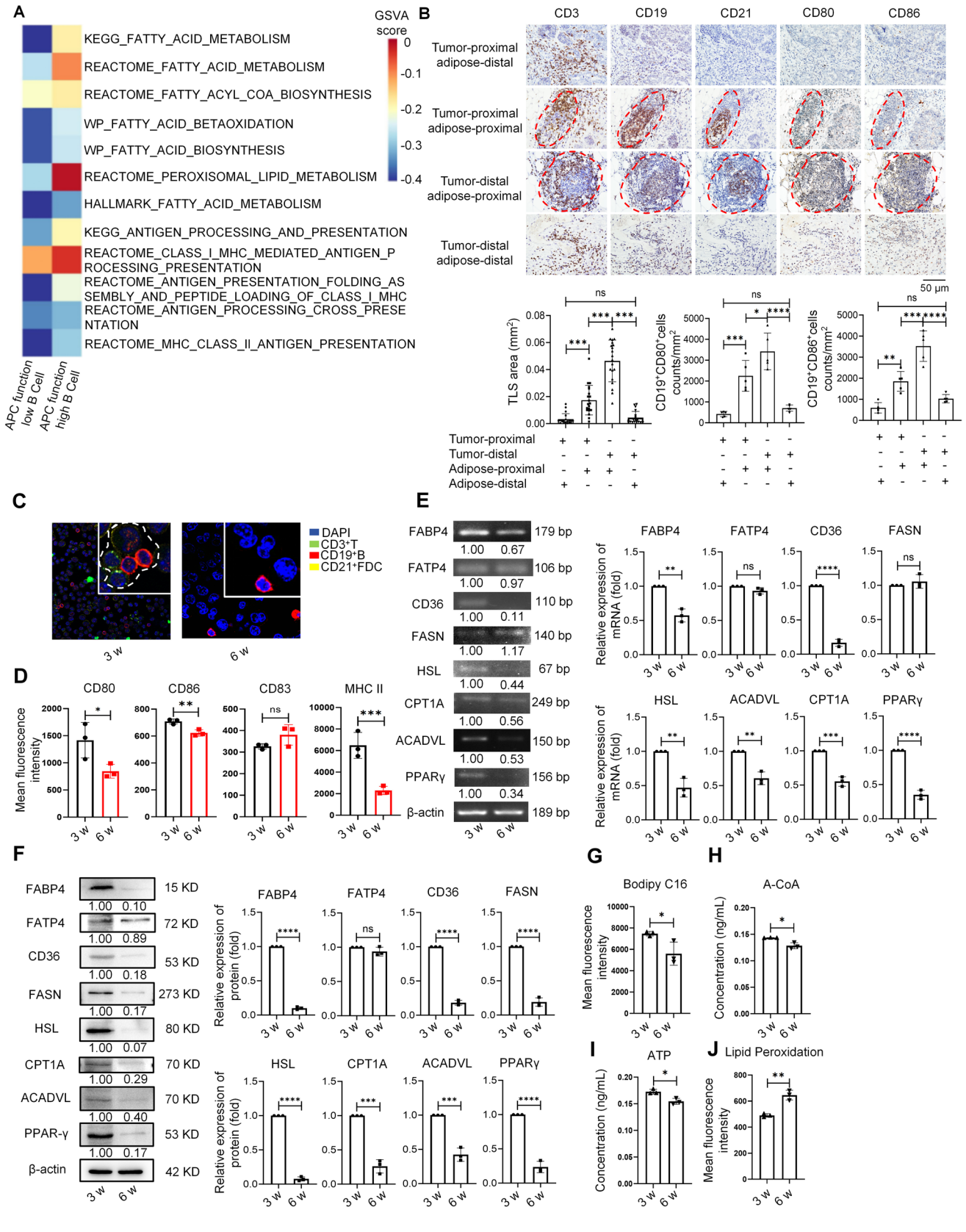
A
GSVA score
KEGG_FATTY_ACID_METABOLISM
REACTOME_FATTY_ACID_METABOLISM
REACTOME_FATTY_ACYL_COA_BIOSYNTHESIS
WP_FATTY_ACID_BETAOXIDATION
WP_FATTY_ACID_BIOSYNTHESIS
REACTOME_PEROXISOMAL_LIPID_METABOLISM
HALLMARK_FATTY_ACID_METABOLISM
KEGG_ANTIGEN_PROCESSING_AND_PRESENTATION
REACTOME_CLASS_I_MHC_MEDIATED_ANTIGEN_PROCESSING_PRESENTATION
REACTOME_ANTIGEN_PRESENTATION_FOLDING_ASSEMBLY_AND_PEPTIDE_LOADING_OF_CLASS_I_MHC
REACTOME_ANTIGEN_PROCESSING_CROSS_PRESENTATION
REACTOME_MHC_CLASS_II_ANTIGEN_PRESENTATION
APC function low B Cell
APC function high B Cell
B
CD3
CD19
CD21
CD80
CD86
Tumor-proximal adipose-distal
Tumor-proximal adipose-proximal
Tumor-distal adipose-proximal
Tumor-distal adipose-distal
50 μm
TLS area (mm²)
CD19⁺CD80⁺cells counts/mm²
CD19⁺CD86⁺cells counts/mm²
Tumor-proximal
Tumor-distal
Adipose-proximal
Adipose-distal
C
DAPI
CD3⁺T
CD19⁺B
CD21⁺FDC
3 w
6 w
D
CD80
CD86
CD83
MHC II
Mean fluorescence intensity
E
FABP4
FATP4
CD36
FASN
HSL
CPT1A
ACADVL
PPARγ
β-actin
Relative expression of mRNA (fold)
F
Relative expression of protein (fold)
G
Bodipy C16
Mean fluorescence intensity
H
A-CoA
Concentration (ng/mL)
I
ATP
J
Lipid Peroxidation

◂**Fig. 2** The APC function of B cells is closely associated with their FA metabolism in metastatic OvCa. **A** GSVA pathway enrichment analysis of APC function low and APC function high B cells in patients with metastatic OvCa (GSE235951, GSE147082 and GSE154600 dataset in the GEO database, n = 13). **B** Representative images of the IHC staining of TLS structure (composed of $CD3^+$T cells, $CD19^+$B cells, and $CD21^+$FDC), CD80, and CD86, respectively, in the area adjacent to or away from tumor or adipose tissues in clinical HGSOC specimens (n = 20 for TLS and n = 5 for CD80 or CD86). Red dashed line area: TLS structure. Magnification × 200. **C** Representative image of lymphoid aggregates (white dashed line area) by immunofluorescent staining in ascites of OvCa mice with 3 w and 6 w in tumor-bearing mice. **D** Mean fluorescence intensity of CD80, CD86, CD83, and MHC class II molecules in ascitic $CD19^+$B cells of OvCa mice were detected by flow cytometry. **E** Comparison of mRNA levels of FA metabolic genes in ascitic B cells in OvCa mice. The relative expression of each gene was calculated using *β*-actin as the internal reference. **F** Protein expression of β-actin and FA metabolic proteins in ascitic B cells in OvCa mice was assessed by WB. *β*-Actin was used as the internal control to calculate the relative expression level of FA metabolic proteins. **G** Mean fluorescence intensity of Bodipy C16 in ascitic B cells of OvCa mice detected by flow cytometry. **H** Expression of A-CoA in ascitic B cells of OvCa mice detected by ELISA. **I** Expression of ATP in ascitic B cells of OvCa mice detected by ELISA. **J** Mean fluorescence intensity of intracellular oxidized lipid in ascitic B cells of OvCa mice detected by flow cytometry. **I** Comparison of mRNA levels of FA metabolic genes in ascitic B cells in OvCa mice. The relative expression of each gene was calculated using *β*-actin as the internal reference. Data are presented as the mean ± SD of three independent experiments. FA, fatty acid; TLS, tertiary lymphoid structure. *p < 0.05, **p < 0.01, ***p < 0.001, ****p < 0.0001, ns, not significant

preliminarily verify this correlation, we conducted immunohistochemical (IHC) staining on HGSOC clinical specimens targeting TLS markers (including $CD3^+$T cells, $CD19^+$B cells, and $CD21^+$FDC) (n = 20) and APC function markers (including CD80, CD86) (n = 5). We found that in the following four different tissue localization groups, the expression levels of APC functional markers and the TLS area decreased successively: (1) tumor-distal/adipose-proximal group, (2) tumor-proximal/adipose-proximal group, (3) tumor-distal/adipose-distal group, and (4) tumor-proximal/adipose-distal group (Fig. 2B). These data suggested that the APC function of B cells and TLS structure are closely associated with the adipocyte-rich microenvironment in OvCa patients.

To further explore the correlation between APC function of B cells and their FA metabolism within TME, we established a metastatic OvCa mouse model and focused on the ascitic B cells (AS-Bs). Interestingly, we found the existence of the lymphoid aggregates in the ascites in 3-w tumor-bearing mice (3 weeks after intraperitoneal injection of ID8) [5, 28, 29]. However, the lymphoid aggregates was not detected in the ascites in 6 w tumor-bearing mice (6 weeks after intraperitoneal injection of ID8) (Fig. 2C). Meanwhile, the median fluorescence intensity (MFI) of CD80 and MHC II in AS-Bs decreased as OvCa progressed, whereas those of CD86 and CD83 (the marker for activation of B cells) did not show significant changes (Fig. S2 C and Fig. 2D). Then, we examined the representative genes in FA metabolism of AS-Bs. The mRNA and protein levels of the main FA uptake genes including FABP4 and CD36, lipolysis genes including HSL, and transport genes including CPT1A, and *β*-oxidization genes including ACADVL, and nuclear transcription factor gene PPARγ, were significantly downregulated as OvCa progressed (Fig. 2E, F). However, FATP4 did not show significant changes. Both APC functions and FA metabolism of AS-Bs decreased with the progression of metastatic OvCa, suggesting that FA metabolism may be closely related to the APC functions of AS-Bs.

Furthermore, we detected the FA content and its metabolic products in AS-Bs and ascites-derived tumor cells The intracellular FA content and lipid peroxidation levels were assessed by BODIPY C16 and C11 uptake assays, and the levels of acetyl-CoA (A-CoA) and ATP were measured by ELISA. The results showed that AS-Bs at 6 w after tumor injection had decreased intracellular FA content, lower levels of A-CoA and ATP (Fig. S2 D, Fig. 2G–I), and significantly higher lipid peroxidation levels compared with those at 3 w (Fig. S2 E, Fig. 2J). Meanwhile, we found that intracellular FA content, A-CoA, and ATP levels in tumor cells at 6 w after tumor injection were significantly higher than those at 3 w after tumor injection (Fig. S2 F–G). These results indicate that ascites-derived tumor cells may compete for FA uptake, leading to dysfunction in AS-Bs FA metabolism. In addition, the decreased FA metabolism of AS-Bs may be a key driver of their impaired APC function.

B cells are not a homogeneous subpopulation of cells and the identity and diversity of B cells might evolve during tumor growth. To examine the changes in B cell subsets during tumor progression, we examined the changes in the proportions of B cell subsets—including naïve B cells ($CD19^+IgD^+CD27^-$), unswitched memory B cells ($CD19^+IgD^+CD27^+$), switched memory B cells ($CD19^+IgD^-CD27^+$) and regulatory B cells ($CD19^+IL\text{-}10^+$)—in the ascites of mice at 3 w and 6 w after intraperitoneal injection of ovarian cancer cells [30]. The results showed that, compared with the 3 w time point, none of the B cell subsets in the ascites changed at 6 w, indicating that in our mouse model, the alteration in B cell APC function during tumor progression is not associated with changes in B cell subset composition (Fig. S2H-I).

The APC function and resulting anticancer immunity of B cells can be enhanced by oleic acid (OA) via reprogramming FA metabolism in vitro

The above results have already indicated that the APC function of B cells in metastatic OvCa is closely positively correlated with its FA metabolism. Then, can the APC function of B cells be enhanced by reprogramming its FA metabolism

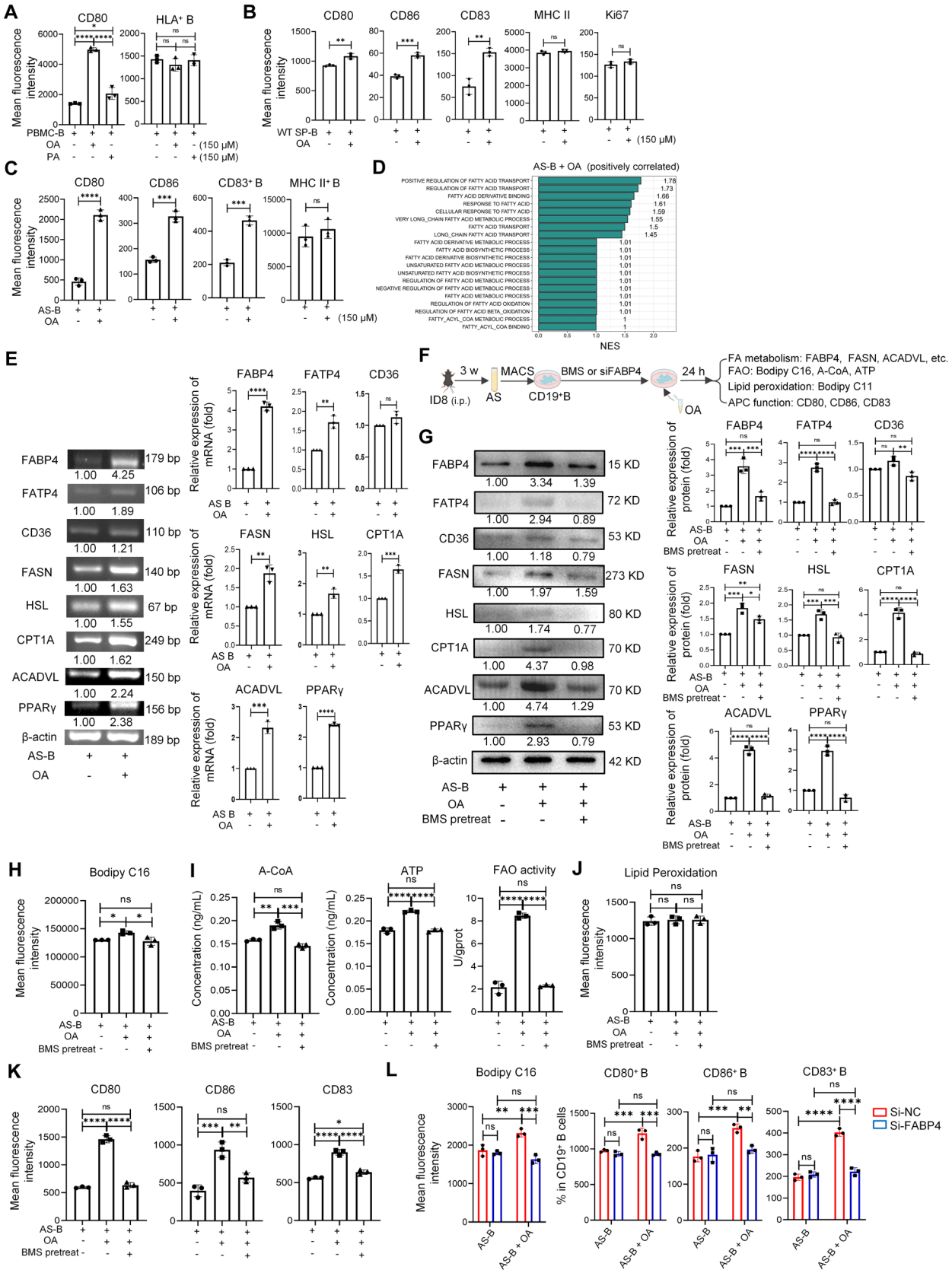
A
CD80
HLA+ B
Mean fluorescence intensity
PBMC-B
OA
PA
(150 μM)
B
CD80
CD86
CD83
MHC II
Ki67
WT SP-B
C
CD80
CD86
CD83+ B
MHC II+ B
AS-B
D
AS-B + OA (positively correlated)
POSITIVE REGULATION OF FATTY ACID TRANSPORT
REGULATION OF FATTY ACID TRANSPORT
FATTY ACID DERIVATIVE BINDING
RESPONSE TO FATTY ACID
CELLULAR RESPONSE TO FATTY ACID
VERY LONG_CHAIN FATTY ACID METABOLIC PROCESS
FATTY ACID TRANSPORT
LONG_CHAIN FATTY ACID TRANSPORT
FATTY ACID DERIVATIVE METABOLIC PROCESS
FATTY ACID BIOSYNTHETIC PROCESS
FATTY ACID DERIVATIVE BIOSYNTHETIC PROCESS
UNSATURATED FATTY ACID METABOLIC PROCESS
UNSATURATED FATTY ACID BIOSYNTHETIC PROCESS
REGULATION OF FATTY ACID METABOLIC PROCESS
NEGATIVE REGULATION OF FATTY ACID METABOLIC PROCESS
FATTY ACID METABOLIC PROCESS
REGULATION OF FATTY ACID OXIDATION
REGULATION OF FATTY ACID BETA_OXIDATION
FATTY_ACYL_COA METABOLIC PROCESS
FATTY_ACYL_COA BINDING
NES
E
FABP4
FATP4
CD36
FASN
HSL
CPT1A
ACADVL
PPARγ
β-actin
Relative expression of mRNA (fold)
F
3 w
ID8 (i.p.)
AS
MACS
CD19+B
BMS or siFABP4
24 h
OA
FA metabolism: FABP4, FASN, ACADVL, etc.
FAO: Bodipy C16, A-CoA, ATP
Lipid peroxidation: Bodipy C11
APC function: CD80, CD86, CD83
G
Relative expression of protein (fold)
BMS pretreat
H
Bodipy C16
I
A-CoA
ATP
FAO activity
Concentration (ng/mL)
U/gprot
J
Lipid Peroxidation
K
L
Bodipy C16
CD80+ B
CD86+ B
CD83+ B
% in CD19+ B cells
Si-NC
Si-FABP4

◂**Fig. 3** The APC function and resulting anticancer immunity of B cells can be enhanced by oleic acid (OA) via reprogramming FA metabolism in vitro. **A** Mean fluorescence intensity of CD80 and MHC Class II molecules in $CD19^+$B cells from peripheral blood of healthy volunteers (n = 3) treated with OA and PA (both 150 μM), respectively. **B** Mean fluorescence intensity of CD80, CD86, CD83, MHC Class II molecules, and Ki67 in splenic $CD19^+$B cells of WT mice treated with 150 μM OA. **C** Mean fluorescence intensity of CD80, CD86, CD83, and MHC Class II molecules in ascitic $CD19^+$B cells from 3 w OvCa-bearing mice when treated with 150 μM OA. **D** Analysis of FA metabolism-related signaling pathways based on RNA-seq results. GSEA was used to analysised the FA metabolic pathways. **E** Comparison of mRNA levels of main FA metabolic genes in ascitic B cells from 3 w tumor-bearing mice when treated with 150 μM OA. The relative expression of each gene was calculated using β-actin as the internal reference. **F** Experimental scheme to detect the influence of inhibiting OA uptake on ascitic B cells. **G** Comparison of protein expressions of main FA metabolic molecules in 3 w OvCa-bearing mouse ascitic B cells pretreated with BMS and treated with OA. β-Actin was used as the internal control to calculate the relative expression level of the main FA metabolic molecules. **H** Mean fluorescence intensity of Bodipy C16 in 3 w OvCa-bearing mouse ascitic B cells pretreated with BMS and treated with OA was detected by flow cytometry. **I** The expression of A-CoA, ATP and the FAO activity in 3 w OvCa-bearing mouse ascitic B cells pretreated with BMS treated with OA was detected by ELISA. **J** Mean fluorescence intensity of intracellular oxidized lipid in 3 w OvCa-bearing mouse ascitic B cells pretreated with BMS and treated with OA was detected by flow cytometry. **K** Mean fluorescence intensity of CD80, CD86, and CD83 in 3 w OvCa-bearing mouse ascitic $CD19^+$B cells pretreated with BMS and treated with OA was detected by flow cytometry. **L** Mean fluorescence intensity of Bodipy C16, CD80, CD86 and CD83 in FABP4-knockdown $CD19^+$B cells, which are from the ascites of 3 w OvCa-bearing mice, treated with OA, was detected by flow cytometry. PBMC, peripheral blood mononuclear cell; SP, spleen; AS, Ascites; OA, oleic acid; PA, palmitic acid; BMS, BMS309403. Data are presented as the mean ± SD of three independent experiments. *$p < 0.05$, **$p < 0.01$, ***$p < 0.001$, ****$p < 0.0001$, ns, not significant

within TME? To address this question, we first treated B cells from the peripheral blood of healthy volunteers with a typical unsaturated FA (oleic acid, OA) and saturated FA (palmitic acid, PA) for 24h, respectively. We found that both FAs significantly increased the MFI of CD80 in $CD19^+$B cells (Fig. S3A and Fig. 3A) and did not cause changes in the MFI of MHC II. Based on Fig. 3A, we chose OA as the FA candidate to promote the APC functions of B cells. Then, we applied splenic B cells (SP-Bs) from wild-type (WT) C57BL/6 mice to conduct above experiments. Similar results were obtained. In detail, OA increased the MFI of CD80, CD86, and CD83 in $CD19^+$ B cells and did not affect the MFI of MHC II or Ki67 (Fig. S3 B and Fig. 3 B), indicating that OA could promote APC function and activation of B cells via costimulatory molecules, not affecting the proliferation. In addition, we examined changes in the proportions of B cell subsets derived from peripheral blood mononuclear cells (PBMCs) and splenocytes of wild-type C57BL/6 mice following treatment with OA or PA. The results showed that treatment with OA or PA did not change the proportions of B cell subsets in either PBMC- or SP-derived B cells (Fig. S3C-D). Subsequently, we used the AS-Bs obtained from OvCa-bearing and confirmed a similar conclusion as Fig. 3B (Fig. 3C). We also carried out the dose–effect and time-effect experiments and confirmed 150 μM and 24h as the optimal concentration and time for OA treatment (Fig. S3E).

As mentioned earlier, FA metabolism involves many steps, and each step has many molecules. Which molecule plays a key role in OA-induced remodeling of FA metabolism, thereby enhancing the APC function of B cells within the TME? To address this question, we conducted experiments using AS-Bs from OvCa-bearing mice (3 w post-tumor loading). We treated AS-Bs with OA meanwhile treated AS-Bs with PBS as the control. After 24h of treatment, RNA was extracted from both the OA-treated and control groups for subsequent RNA sequencing (RNA-seq). The results revealed that, compared with the control group, OA-treated AS-Bs exhibited a significant upregulation of FA metabolic pathways. These included positive regulation of fatty acid transport, regulation of fatty acid transport, etc. (Fig. 3D). These findings suggest that the pathway of FA transport (including FA uptake) may play an important role in the OA-induced reprogramming of FA metabolism in AS-Bs. To validate the above bioinformatics analysis results, we detected the mRNA levels of genes related to FA metabolism in AS-Bs using RT-PCR experiments (Fig. 3E). Additionally, to better mimic the interaction between $CD4^+$T cells and B cells within the TME, B cells were treated with CD40L and IL-4. The results showed that after AS-Bs exhibited significant upregulation of key FA metabolism genes (such as FABP4, FATP4, FASN, HSL, CPT1A, and ACADVL) and the important lipid metabolism transcription factor PPARγ, while the expression of CD36 remained unchanged. Notably, FABP4, a core regulatory factor in FA metabolism including FA uptake, showed the most significant increase (Fig. 3E).

Subsequently, to verify the crucial role of FABP4 in OA-induced enhancement of APC function of AS-Bs mentioned above, we first conducted experiments using CD40L, IL-4, and the FABP4 inhibitor BMS309403 (BMS), followed by related detection (Fig. 3F). The results of the western blotting assay showed that the molecular proteins involved in FA metabolism in AS-Bs were significantly upregulated after OA treatment and downregulated when pretreated with BMS (Fig. 3G). In addition, we detected the intracellular FA content and lipid peroxidation levels in AS-Bs using BODIPY C16 and C11 uptake assays, and measured the levels of A-CoA, ATP and the FAO activity in B cells using ELISA, respectively. We found that OA treatment significantly upregulated intracellular FA content, A-CoA levels, ATP production and the FAO activity in AS-Bs, while lipid peroxidation levels remained unchanged. After pretreatment

with BMS, the intracellular FA content, the levels of A-CoA and ATP, as well as the FAO activity in AS-Bs, were all downregulated (Fig. S4 B and Fig. 3H–J). Meanwhile, flow cytometry analysis showed that BMS pretreatment blocked the OA-induced upregulation of the MFI of CD80, CD86, and CD83 in $CD19^+$B cells (Fig. S4C and Fig. 3K); neither OA nor BMS treatment altered the proportions of B cell subsets (Fig. S4D). Secondly, we also conducted the experiments using FABP4 siRNA instead of BMS (Fig. S4E). The results showed that, with the same treatment with OA, compared with the control cells (siNC), the knockdown of FABP4 in AS-Bs significantly decreased the intracellular FA content (Fig. S4F and Fig. 3L). Meanwhile, FABP4 knockdown significantly downregulated the MFI of CD80, CD86, and CD83 in $CD19^+$B cells (Fig. S4 F and Fig. 3L). These findings indicate that OA promotes APC functionality of AS-Bs primarily through the FABP4 molecule.

To determine whether enhancing the APC function of B cells within the TME—whose FA metabolism has been reshaped by OA—can ultimately improve anti-tumor immunity, we established an in vitro coculture model. This model consisted of antigen-pulsed AS-Bs, splenic T cells from OvCa-bearing mice, and ID8-Luc cells. We first used antigenic peptides prepared by ID8 cells to pulse AS-Bs obtained from OvCa mice together with OA treatment. Then we mixed the AS-Bs with splenic T cells also from OvCa mice to exert APC functions and finally added ID8-Luc cells as the target cells in the system (Fig. 4). We used flow cytometry to assess AS-Bs CD80/CD86/CD83 expression, ELISA to quantify T cell effector molecules (including IFN-γ, GZMB, TNF-α), and luciferase assays to evaluate T cell cytotoxicity against ID8-Luc cells. The results showed that antigenic peptide stimulation upregulated the MFI of CD80, CD86, and CD83 in $CD19^+$B cells, which was further elevated by OA treatment (Fig. S4 G and Fig. 4B). Among T cell effector molecules in the supernatant, OA treatment induced a significant elevation in TNF-α levels, while IFN-γ and GZMB showed no significant changes (Fig. 4 C). TNF-α upregulation was accompanied by a corresponding about 70% increase in T cell cytotoxicity against ID8-Luc cells, which was reversed by BMS pretreatment. The above results indicate that OA treatment enhanced the APC function of AS-Bs, which in turn improved anticancer immunity in vitro (Fig. 4 D).

The enhanced APC function of AS-Bs by OA in vitro is achieved through H3K27ac-mediated upregulation of PPARγ expression

Subsequently, we investigated the mechanisms by which OA promotes the expression of genes related to the APC function of AS-Bs. Our previous results showed that OA treatment in vitro increased the level of A-CoA in AS-Bs (Fig. 3I). Given that A-CoA serves as the essential acetyl donor for H3K27 acetylation (H3K27ac), an epigenetic modification that reduces chromatin compaction and enhances DNA accessibility for transcription factors, we first examined H3K27ac levels in OA-treated AS-Bs using WB. The results showed that the OA treatment group exhibited significantly elevated H3K27ac levels in B cells compared with the control group (Fig. 5A). Then, we used chromatin immunoprecipitation (ChIP) assays to examine the enrichment of H3K27ac at the promoter regions of APC function-related genes (such as CD80, CD86, and CD83) and the key lipid metabolism transcription factor PPARγ. The results showed that, compared with the control group, H3K27ac was significantly enriched only at the PPARγ promoter region after OA treatment, while H3K27ac enrichment at the promoter region of CD80, CD86, and CD83 showed an upward trend but no significant changes (Fig. 5B). Then, we analyzed the correlation between PPARγ expression and APC functional molecules (such as CD80, CD86, and CD83) in OvCa using sequencing data from 426 OvCa patients in the TCGA database. The results showed a significant positive correlation between PPARγ expression and APC functional molecules (such as CD80, CD86, and CD83) in OvCa (Fig. 5C). These findings suggest that OA treatment enhances the expression of genes related to the APC function of AS-Bs not through direct H3K27ac-mediated regulation, but rather via significant transcription factor PPARγ.

Building on our prior findings that the use of a FABP4 inhibitor and siFABP4 significantly downregulated the OA-enhanced APC function of AS-Bs, we next sought to clarify whether OA could promote the expression of CD80, CD86, and CD83 in AS-Bs via FABP4-PPARγ. We conducted a protein–protein interaction analysis between FABP4, PPARγ, CD80, CD86, and CD83. The results show that FABP4 may influence CD80, CD86, and CD83 expression via PPARγ (Fig. 5D). We next performed a ChIP assay to examine the enrichment of PPARγ at the promoter regions of APC function-related genes, such as CD80, CD86, and CD83. The results demonstrated that OA treatment led to a significant increase in PPARγ enrichment at the promoter regions of CD80, CD86, and CD83 compared with the control group (Fig. 5E). To validate the above results, we pretreated AS-Bs with the PPARγ inhibitor GW9662 and the PPARγ agonist Trog, and then detected the MFI of CD80, CD86, and CD83 in $CD19^+$B cells using flow cytometry. The results showed that the enhancing effects of OA treatment on the MFI of CD80, CD86, and CD83 in $CD19^+$B cells were inhibited by GW9662 (the PPARγ inhibitor, Fig. S5 and Fig. 5F). Additionally, the inhibitory effects of BMS on OA-increased the MFI of CD80, CD86, and CD83 in $CD19^+$B cells were reversed by Trog (the PPARγ agonist, Fig. S5 and Fig. 5F). These findings suggested that OA enhances the expression of genes related to the APC function of AS-Bs by promoting PPARγ expression through H3K27ac-mediated epigenetic regulation.

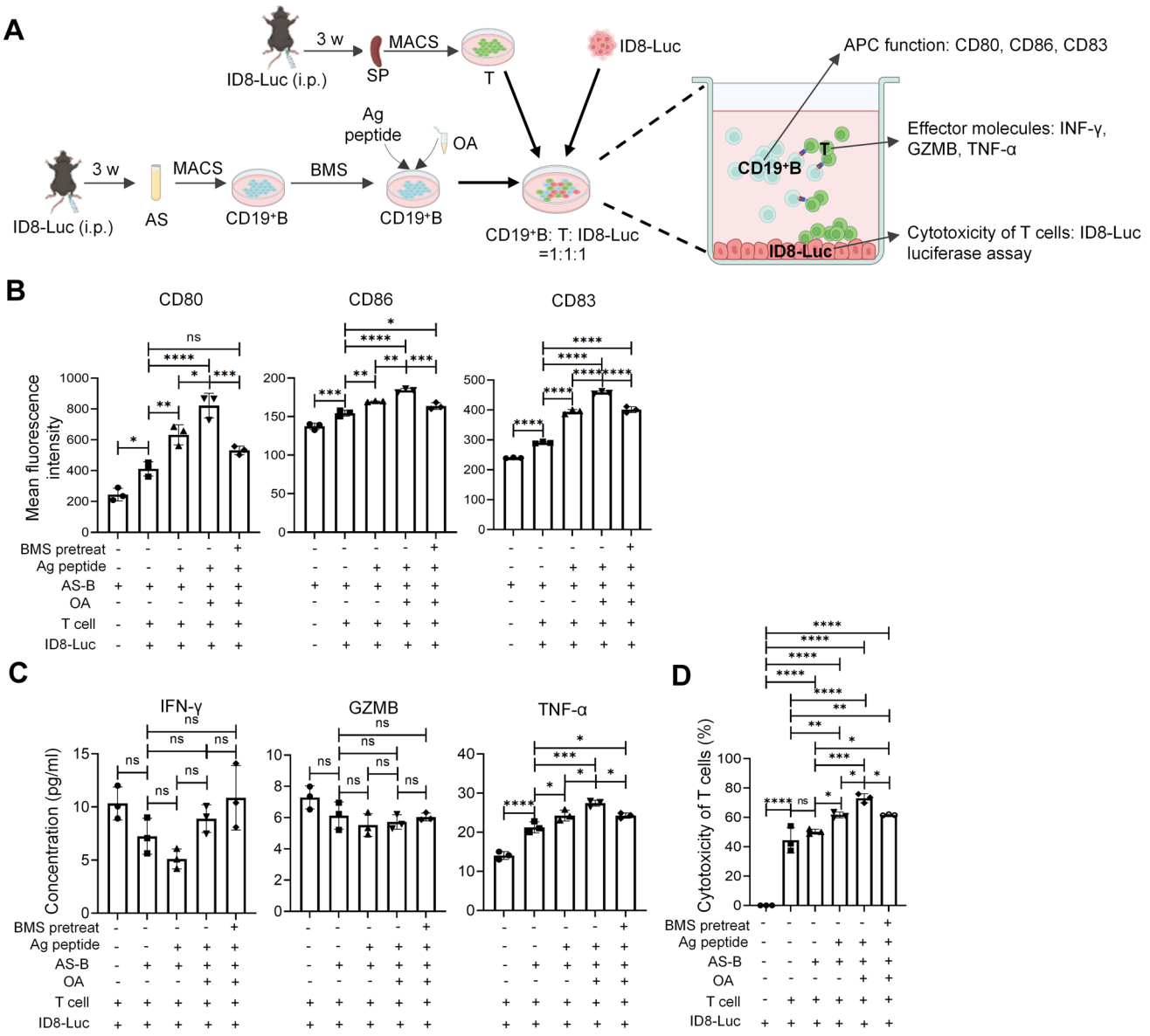

Fig. 4 Reprogramming of the FA metabolism of B cells by OA can improve anticancer immunity in vitro. **A** Experimental scheme to detect the in vitro effects of ascitic B cells treated with OA on anticancer immunity. **B** Mean fluorescence intensity of CD80, CD86, and CD83 in 3 w OvCa-bearing mouse ascitic $CD19^+B$ cells after pulsed with ID8-Luc-cell-prepared antigenic peptides and pretreated with BMS and treated with OA, T cells and ID8-Luc. **C** Levels of IFN-γ, GZMB, and TNF-α in the supernatant of the coculture system constructed by ID8-Luc cells and 3 w OvCa-bearing mouse ascitic B and splenic T cells were detected by ELISA. **D** Cytotoxicity of T cells in the coculture system mentioned above was detected by luciferase assay. AS, Ascites; Ag, Antigen; OA, oleic acid; BMS, BMS309403. Data are presented as the mean ± SD of three independent experiments. *p < 0.05, **p < 0.01, ***p < 0.001, ****p < 0.0001, ns, not significant

The combination of adoptive immunotherapy with APC function-enhanced AS-Bs and low-dose chemotherapy (LDC) improved anticancer immunity in metastatic OvCa mice

To detect whether reprogramming of the FA metabolism of AS-Bs by OA could improve anticancer immunity in vivo, we combined the adoptive transfer of OA-treated AS-Bs (B_{OA}) with chemotherapy (DDP) in the metastatic OvCa mice (Fig. 6A). While chemotherapy remains the primary treatment modality for OvCa, its clinical application is limited by dose-dependent cytotoxicity toward both malignant and normal cells, resulting in significant adverse effects. Consequently, low-dose chemotherapy was strategically selected for subsequent research. Rather than administering OA directly to mice (in vivo intervention), we treated B cells

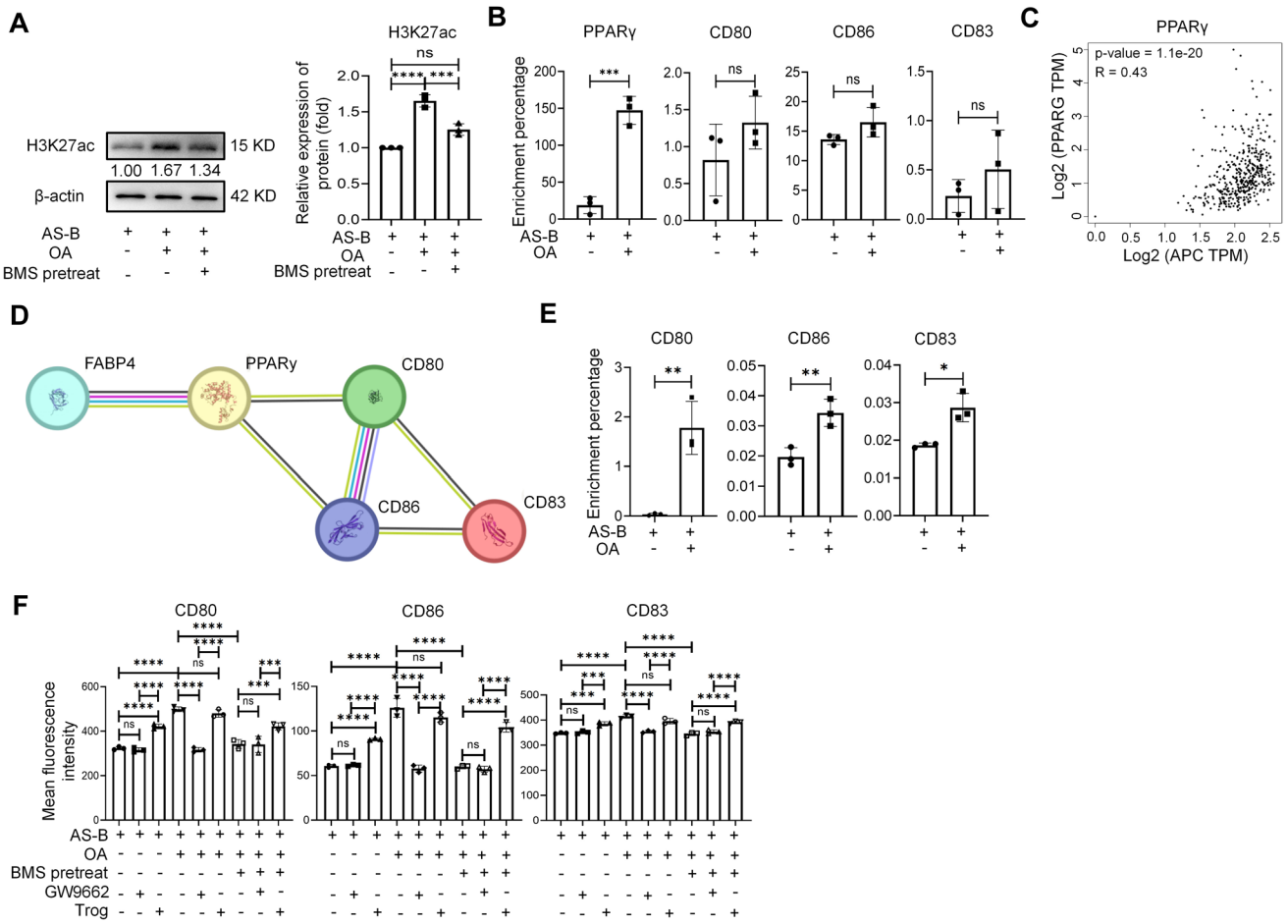

Fig. 5 The enhanced APC function of B cells by OA in vitro is achieved through H3K27ac-mediated upregulation of PPARγ expression. **A** Protein expression of β-actin and H3K27ac in 3 w OvCa-bearing mouse ascitic CD19$^+$B cells pretreated with BMS and treated with OA was assessed by WB. β-Actin was used as the internal control to calculate the relative expression level of H3K27ac. **B** The enrichment percentage of H3K27ac at the PPARγ, CD80, CD86, and CD83 promoter regions was quantified using ChIP-seq analysis. **C** Correlation analysis of PPARγ and APC function-related genes (CD80, CD86, CD83, MHC II) in B cells in OvCa patients in the TCGA database (n = 426). **D** Analysis of protein interaction among FABP4, PPARγ, CD80, CD86, and CD83. **E** The enrichment percentage of PPARγ at the CD80, CD86, and CD83 promoter regions was quantified using ChIP-seq analysis. **F** Mean fluorescence intensity of CD80, CD86, and CD83 in 3 w OvCa-bearing mouse ascitic CD19$^+$B cells pretreated with BMS, GW9662/Trog, and treated with OA was detected by flow cytometry. AS, Ascites; Ag, Antigen; OA, oleic acid; BMS, BMS309403. Data are presented as the mean ± SD of three independent experiments. *p < 0.05, **p < 0.01, ***p < 0.001, ****p < 0.0001, ns, not significant

(isolated from ascites of 3 w OvCa-bearing mice) with OA ex vivo for 24h and then performed adoptive transfer into recipient OvCa mice. To select the optimal injection route for AS-Bs adoptive immunotherapy, we labeled AS-Bs with CM-Dil and performed the in vivo tracing experiment of AS-Bs (Fig. S6A). The results showed that most intraperitoneally injected AS-Bs were detected in the peritoneal lavage fluid, and the intravenously injected AS-Bs were distributed into multiple organs or tissues and mainly circulated into the bone marrow (Fig. S6B). Therefore, we applied intraperitoneal injection for the adoptive transfer of AS-Bs to exert APC functions in TME. At 4 w post-tumor inoculation, bioluminescence imaging and dissection analysis revealed that mice in the combination therapy group (L-DDP + B_{OA}) exhibited significantly reduced tumor burden (Fig. 6B) and fewer abdominal tumor nodules (Fig. 6C) than those in the L-DDP group. Meanwhile, no significant differences were observed between the combination therapy group and the H-DDP group. We then analyzed the ascitic T and B cells. There were many more ascitic CD3$^+$T cells, CD8$^+$T cells, Ki67$^+$CD3$^+$T cells, Ki67$^+$CD8$^+$T cells, CD19$^+$B cells, CD19$^+$CD80$^+$B cells, CD19$^+$CD86$^+$B cells, and lymphoid aggregates in the combination therapy group than those in the other groups (Fig. S7 and Fig. 6D). It is noteworthy that in the analysis of samples presented in Fig. 2, no lymphoid aggregates were observed in the ascites at the 6-w tumor burden time point, compared to the 3 w time point. We also detected the percentages of the cells and the MFI of Ki67,

CD80, CD86, CD83, etc. by flow cytometry (Fig. S8C and Fig. 6E), further confirming the results in Fig. 6D. MFI analysis showed that, in the combination therapy group, the MFI of IL-2, IFN-γ, and GZMB in $CD8^+$ T cells was significantly higher than that in the other groups. CTLA-4, an important immune negative regulatory molecule, in $CD8^+$T cells from the mice of the combination therapy group was lower than that in other groups (Fig. S8D and Fig. 6F). A parallel survival experiment demonstrated that the combination of L-DDP and B_{OA} significantly extended the survival time of mice (MS: 101 d) compared with the L-DDP group (MS: 90 d) (Fig. 6G). There was no significant difference between the combination therapy group and the H-DDP group (MS:95 d). The above data confirmed that the combination of APC function-enhanced AS-Bs adoptive transfer with LDC improved anticancer immunity in metastatic OvCa mice.

Discussion

Metabolic reprogramming is an essential driving force for the functional differentiation of B cells [31, 32]. The present study demonstrated that in vitro oleic acid (OA) treatment of AS-Bs isolated from tumor-bearing mice promotes their APC function through FA metabolic reprogramming, which in turn improves tumor cell killing mediated by T cells. Mechanistically, we found that OA enhanced the APC function of AS-Bs through H3K27ac-mediated upregulation of PPARγ expression. Our study also demonstrated that adoptive immunotherapy with APC function-enhanced AS-Bs combined with low-dose chemotherapy (LDC) significantly prolongs survival in mouse models of metastatic ovarian cancer (OvCa).

Eighty percent of HGSOC patients develop severe ascites, which is rich in fatty acids [13, 14]. However, in the OvCa mouse model, with tumor progression and ascites accumulation, FA metabolism of ascitic B cells exhibited a decreasing trend. Xu et al. found that elevated lipid oxidation in TME increases the uptake of oxidized lipids by $CD8^+$ tumor-infiltrating lymphocytes ($CD8^+$TILs), thereby promoting lipid peroxidation accumulation and inducing functional impairments in $CD8^+$TILs [33]. We also observed elevated lipid peroxidation and reduced ATP levels in AS-Bs during OvCa progression in the mouse model, whereas in vitro OA treatment did not affect the lipid peroxidation levels of AS-Bs. These fundings suggest that in TME, B cells are unable to use FAs to meet their cellular energy demands, which may reduce the expression of genes related to the APC function (such as CD80, CD86, and CD83), impairing the APC function of B cells within TME.

FA metabolism plays a crucial role in regulating B cell activation, differentiation, and functional modulation. The principal FA transport proteins involved include FABPs, FATPs, and CD36. Woong-Jai Won et al. reported that in a normal C57BL/6 mouse B cells model with LPS immunization, CD36-mediated FA uptake supports antibody production in B cells [34]. Shuhei Kobayashi et al. reported that FABP3 deficiency impairs B cells activation and plasma cell differentiation in the same murine model [35]. In this study, using both FABP4 inhibitors and endogenous knockdown approaches, we demonstrated that OA-treated AS-Bs of OvCa-bearing mice primarily rely on FABP4-mediated FA uptake to sustain their APC function. The underlying mechanisms warrant further investigation. PPARγ acts as a master transcriptional regulator of FA metabolism [36]. Our results show that in vitro, OA enhances H3K27 acetylation levels by promoting FAO, thereby increasing chromatin accessibility, upregulating PPARγ expression, boosting the expression of APC-related molecules (such as CD80, CD86) and ultimately improving the APC function of AS-Bs.

In the in vitro coculture system of this study, the enhancement of T cell-mediated tumor cytotoxicity by OA-treated B cells was accompanied by a significant increase in the level of TNF-α in the culture supernatant, whereas the levels of IFN-γ and GZMB showed no significant change. This observation suggests that under these conditions, the T cell effector response elicited by OA-treated B cells may preferentially kill tumor cells via TNF-α-mediated cell death pathways (e.g., apoptosis/necroptosis), rather than the classical perforin/granzyme pathway[37, 38]. TNF-α, a key effector molecule produced by both activated $CD4^+$ and $CD8^+$ T cells, can directly induce target cell death, providing a plausible explanation for the observed increase in tumor cell killing [39, 40]. Future studies could employ specific blockade of signaling pathways such as TNF-α to further dissect the precise contribution and synergistic relationships of different effector molecules in the antit-umor immunity elicited by this combination therapy.

While our study elucidates the immunometabolic mechanisms of OA action on B cells in vitro, an important translational question arises: could an oleic acid-rich diet modulate B cell function and anti-tumor immunity in vivo? Existing evidence suggests a plausible link. Epidemiological and clinical studies have associated Mediterranean diets, rich in OA from sources like olive oil, with reduced cancer risk and improved outcomes, which may partly be attributed to immunomodulatory effects [41]. In animal models, diets high in OA have been shown to influence immune cell profiles and function. For instance, a study by Carrillo et al. (2012) demonstrated that feeding mice an OA-enriched diet altered lymphocyte distribution and activation states in secondary lymphoid organs [42]. More specifically, research by Moro-García et al. (2013) indicated that oleic acid can influence human lymphocyte activation and function, potentially through modulation of membrane fluidity and signaling pathways [43]. Although direct evidence linking OA-rich

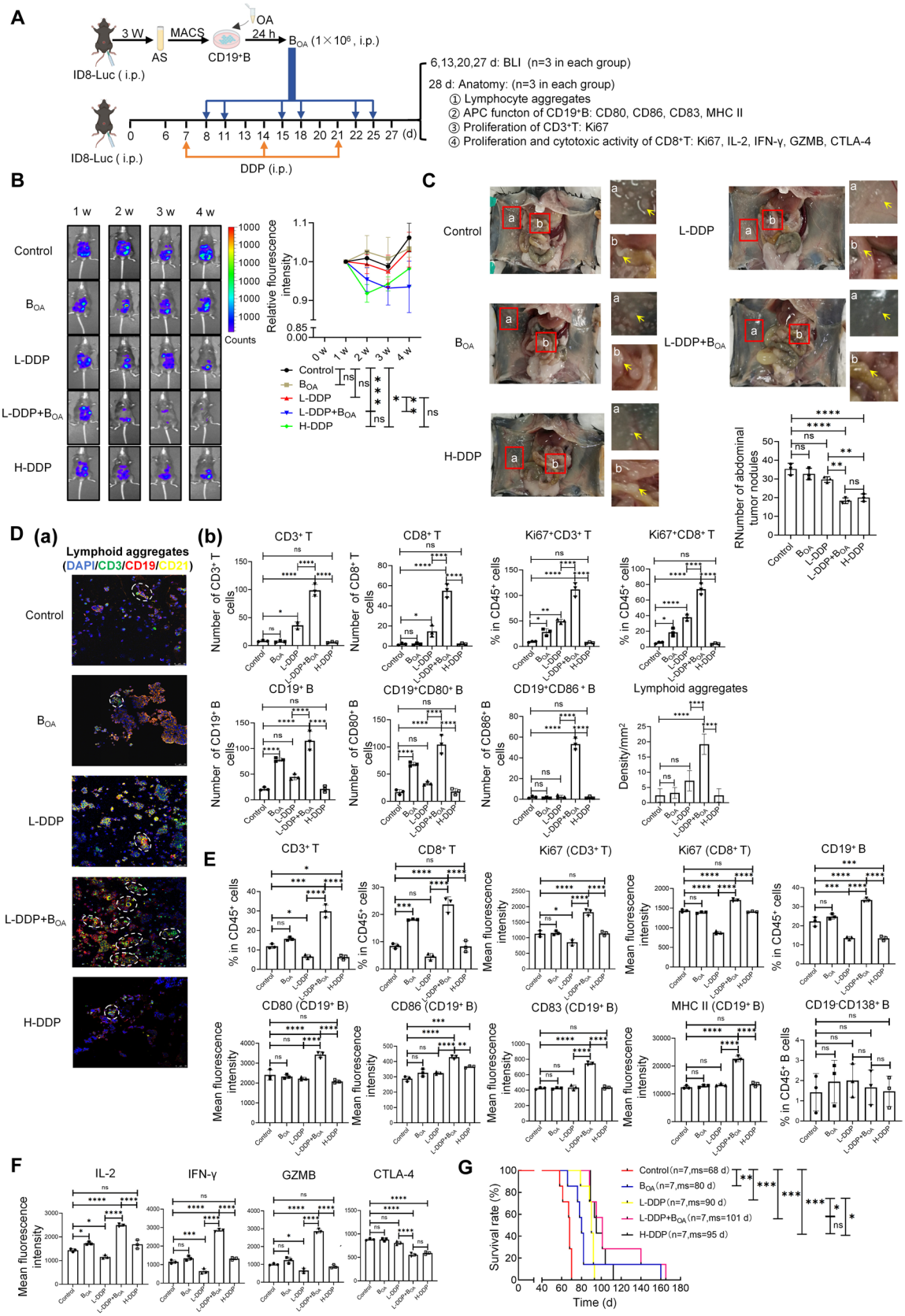
A
3 W
MACS
AS
CD19⁺B
OA
24 h
B_OA (1×10⁶, i.p.)
ID8-Luc (i.p.)
6,13,20,27 d: BLI (n=3 in each group)
28 d: Anatomy: (n=3 in each group)
① Lymphocyte aggregates
② APC functon of CD19⁺B: CD80, CD86, CD83, MHC II
③ Proliferation of CD3⁺T: Ki67
④ Proliferation and cytotoxic activity of CD8⁺T: Ki67, IL-2, IFN-γ, GZMB, CTLA-4
0 6 7 8 11 13 14 15 18 20 21 22 25 27 (d)
DDP (i.p.)
B
1 w 2 w 3 w 4 w
Control
B_OA
L-DDP
L-DDP+B_OA
H-DDP
Counts
Relative flourescence intensity
C
Control
L-DDP
B_OA
L-DDP+B_OA
H-DDP
RNumber of abdominal tumor nodules
D (a)
Lymphoid aggregates
(DAPI/CD3/CD19/CD21)
(b)
CD3⁺ T
CD8⁺ T
Ki67⁺CD3⁺ T
Ki67⁺CD8⁺ T
CD19⁺ B
CD19⁺CD80⁺ B
CD19⁺CD86⁺ B
Lymphoid aggregates
E
CD3⁺ T
CD8⁺ T
Ki67 (CD3⁺ T)
Ki67 (CD8⁺ T)
CD19⁺ B
CD80 (CD19⁺ B)
CD86 (CD19⁺ B)
CD83 (CD19⁺ B)
MHC II (CD19⁺ B)
CD19⁻CD138⁺ B
F
IL-2
IFN-γ
GZMB
CTLA-4
Mean fluorescence intensity
G
Survival rate (%)
Time (d)
Control(n=7,ms=68 d)
B_OA(n=7,ms=80 d)
L-DDP(n=7,ms=90 d)
L-DDP+B_OA(n=7,ms=101 d)
H-DDP(n=7,ms=95 d)

◂**Fig. 6** The combination of adoptive immunotherapy with APC function-enhanced B cells and LDC improved anticancer immunity in metastatic OvCa mice. **A** Experimental scheme to evaluate the effects of combining adoptive immunotherapy with APC function-enhanced B cells and LDC in metastatic OvCa mice. **B** Representative BLI images and comparison of OvCa progression in each group (n = 3). **C** Representative images (**a**) and the number of tumor nodules (**b**) in the abdominal wall of mice in each group (n = 3). Areas marked by yellow dashed lines: Representative tumor nodules in the abdominal wall. **D** (a) Representative images of lymphoid aggregates (composed of $CD3^+$T cells, $CD19^+$B cells, and $CD21^+$FDC) in the ascitic cells of mice in each group. (b) Comparison of the amount of $CD3^+$T, $CD8^+$T, $Ki67^+CD3^+$T, $Ki67^+CD8^+$T, $CD19^+$B, $CD80^+$B, $CD86^+$B, and lymphoid aggregates respectively in the ascitic cells of mice in each group (n = 3) in frozen sections detected by immunofluorescence. **E** Comparison of the proportion of $CD3^+$T, $CD8^+$T, $CD19^+$B, $CD19^-CD138^+$B cells, mean fluorescence intensity of Ki67 in $CD3^+$T and $CD8^+$T, and mean fluorescence intensity of CD80, CD86, CD83, MHC II in $CD19^+$B, respectively, in ascitic cells of each group of mice (n = 3) detected by flow cytometry. **F** Mean fluorescence intensity values of IL-2, IFN-γ, GZMB, and CTLA-4 in $CD8^+$T cells, respectively. **G** Kaplan Meier analysis of survival time of each group of mice (n = 7). LDC, low-dose chemotherapy; B_{OA}, B cells that have been treated with OA for 24h; L-DDP, low-dose DDP (1 mg/kg); H-DDP, high-dose DDP (2 mg/kg); BLI, bioluminescence imaging. *p < 0.05, **p < 0.01, ***p < 0.001, ****p < 0.0001, ns, not significant

diets to enhanced B cell APC function in cancer is still evolving, our finding that OA reprograms B cell metabolism via PPARγ to upregulate costimulatory molecules (CD80/86) provides a mechanistic hypothesis for such dietary effects. It is conceivable that dietary OA, by similarly promoting a metabolic and transcriptional program favoring FA oxidation and PPARγ activity in B cell precursors or mature B cells within lymphoid tissues or the TME, could sustain their APC capacity and support TLS formation. Future studies employing controlled OA dietary interventions in tumor-bearing models are warranted to directly test this hypothesis and to determine if nutritional strategies could adjuvant B cell-based immunotherapies.

In recent years, adoptive immunotherapies based on B cells have gradually attracted attention, mainly focused on activating B cells via stimulating CD40/CD40L signaling [44, 45]. However, once B cells activate, proliferate, and differentiate into plasma cells, they will lose APC functions due to the disappearance of B cell receptor (BCR), MHC class II molecules, and costimulatory molecules. Therefore, taking full advantage of the APC function of B cells before they differentiate into plasma cells may be a better therapeutic strategy [46]. The present study emphasized the influence of reprogramming FA metabolism on the APC functions of AS-Bs without causing changes in plasma cells (Fig. 6E).

Up to now, chemotherapy remains the primary treatment for ovarian cancer [20]. In recent years, low-dose chemotherapy (LDC) has attracted increasing attention. LDC can induce cancer cell apoptosis and release intracellular antigens, including tumor-specific antigens and tumor-associated antigens, which can be taken up by APCs. Céline M. Laumont et al. (Cancer Cell, 2023) reported that BCRs on B cells within TME primarily bind endogenous antigens rather than exogenous antigens [47]. LDC further promotes the maturation and function of dendritic cells and upregulates the expression of surface APC-related molecules (such as MHC II and CD86.) [48], thereby more effectively activating T cells. By reducing chemotherapy dosage to mitigate side effects and optimizing synergistic efficacy, the combination of LDC with immune checkpoint blockade (ICB) has demonstrated encouraging outcomes across multiple tumor models and clinical trials [49, 50]. In this study, the combination of LDC with adoptive immunotherapy using APC -function-enhanced AS-Bs significantly prolonged survival in metastatic OvCa mouse models. However, further research is required to optimize LDC dosing and combination strategies for clinical translation.

Recent studies have demonstrated that tertiary lymphoid structures (TLS) play a pivotal role in anti-tumor immunity and are associated with a favorable prognosis [51–53], although the prognostic effect may be influenced by the location and maturation stage of the TLS [54]. Over the past five years, emerging evidence has linked glucose, amino acid, and lipid metabolism to TLS formation. Notably, lipid metabolism promotes TLS assembly by expanding $CD20^+$B cell populations. In this study, we identified a significant association between TLS (the primary niche for B cells) and FA metabolism. Our analysis of RNA-seq data from 426 OvCa patients revealed positive correlations between TLS signature genes and FA metabolic pathway genes. Furthermore, immunohistochemical staining of clinical OvCa specimens (n = 20) demonstrated a progressive decrease in both TLS area and expression of B cells APC functional markers (CD80, CD86) across four distinct tissue localization groups, in sequence. (1) tumor-distal/adipose-proximal, (2) tumor-proximal/adipose-proximal, (3) tumor-distal/adipose-distal, and (4) tumor-proximal/adipose-distal. These results suggest that TLS formation and APC function of B cells in the adipocyte-rich TME are lipid-dependent. In OvCa mouse models, the combination therapy of adoptive immunotherapy using OA-treated AS-Bs (enhanced APC function) and LDC showed significantly increased lymphoid aggregates in ascites and elevated expression of B cell APC functional markers (CD80, CD86, and CD83) compared with other control groups. These results suggest that in vitro OA-mediated reprogramming of B cells FA metabolism promotes B cell APC function and enhances TLS formation, but the underlying dynamic mechanisms require further investigation.

In summary, our study demonstrates that in vitro OA treatment promotes the APC function of B cells from OvCa mice via metabolic reprogramming. Mechanistically, OA enhances the APC function of B cells through

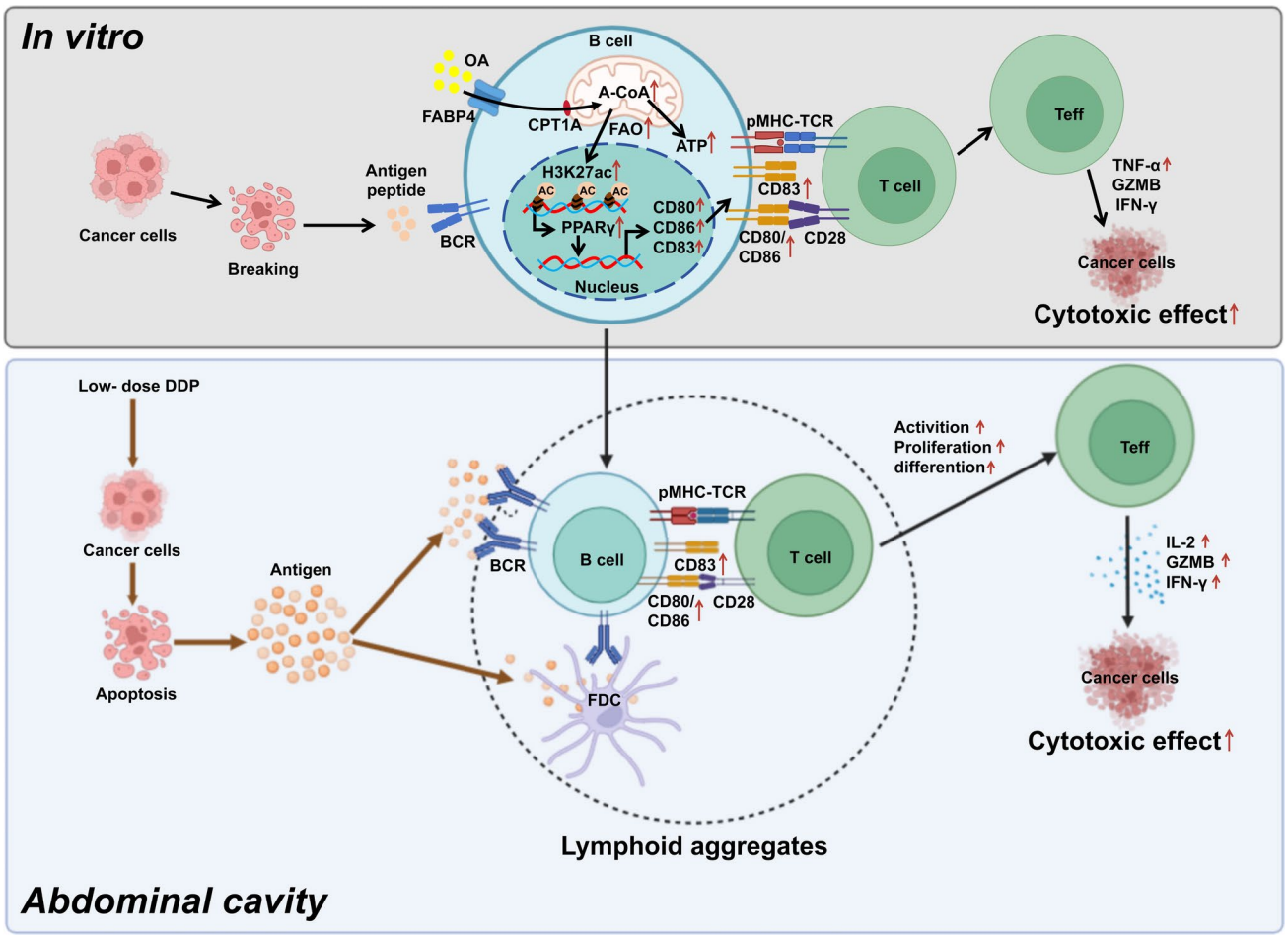

Fig. 7 The mechanism diagram of combining adoptive immunotherapy with APC-function-enhanced B cells and LDC improves anticancer immunity in metastatic OvCa mice. In vitro, OA enhances the expression of CD80/CD86/CD83 of B cells through the H3K27ac-mediated upregulation of PPARγ expression. Then, the B cells are adoptively transferred into the abdominal cavity of metastatic OvCa mice. In the abdominal cavity, LDC facilitates the APC function of the transferred B cells by causing apoptosis of cancer cells. The transferred B cells promote the activation, proliferation, and differentiation of T cells, which release higher levels of effector molecules (IL-2, GZMB, and IFN-γ, etc.), and facilitate the formation of lymphoid aggregates, finally improving anticancer immunity. LDC, low-dose chemotherapy

a FAO-dependent increase in histone H3K27 acetylation, which subsequently upregulates of PPARγ expression within TME. The therapeutic combination of transferring APC function-enhanced B cells with LDC significantly improved anti-tumor immunity in metastatic ovarian cancer models (Fig. 7). These findings provide novel mechanistic insights for developing B cell-based immunotherapies.

Supplementary Information The online version contains supplementary material available at https://doi.org/10.1007/s00262-026-04387-y.

Acknowledgement Not applicable.

Author contributions Haoke Zhang contributed to conceptualization, data curation, formal analysis, validation, investigation, visualization, methodology, writing–original draft, and writing–review and editing. Chunyan Yu contributed to validation, investigation, visualization, methodology, and writing–review. Wei Du contributed to conceptualization, data curation, formal analysis, and editing. Huiyang Li and Zihe Liu contributed to formal analysis, validation, investigation, and visualization. Xueying Li, Bo Wang, Yuhan Yue, Yuqing Ouyang, and Hongmei Wang contributed to investigation. Haixia Wu, Hong Zhang, Yaru Liu, Siyu Cai, Jianchun Yu, Boyu Ji, and Xiaofan Feng contributed to methodology. Weimin Deng contributed to conceptualization, resources, supervision, funding acquisition, project administration, and writing–review and editing.

Funding This research was supported by grants from the National Natural Science Foundation of China (82273340 to W. Deng) and the Beijing-Tianjin-Hebei Basic Research Cooperation Project (20JCZXJC00140 to W. Deng).

Data availability All data generated or analyzed during this study are available from the corresponding author on reasonable request.

Declarations

Conflict of interest The authors declare no conflict of interest.

Ethics approval All the procedures related to patient specimens were conducted following the ethical standards of Tianjin Central Hospital of Gynecology Obstetrics (Ethical approval number 2017KY009) and with the 1964 Helsinki Declaration and its later amendments or comparable ethical standards. Written informed consent was obtained from all the participants before participation in the study. All animal experiments were performed following the protocol approved by the Animal Ethical and Welfare Committee (AEWC) of Tianjin Medical University (Protocol number SYXK 2019–0004).

Consent for publication The authors agree to the publication in the journal.

References

1. Paijens ST, Vledder A, de Bruyn M et al (2021) Tumor-infiltrating lymphocytes in the immunotherapy era. Cell Mol Immunol 18:842–859. https://doi.org/10.1038/s41423-020-00565-9
2. Lu Y, Zhao Q, Liao JY et al (2020) Complement signals determine opposite effects of B Cells in chemotherapy-induced immunity. Cell 180:1081–97.e24. https://doi.org/10.1016/j.cell.2020.02.015
3. Nielsen JS, Sahota RA, Milne K et al (2012) CD20+ tumor-infiltrating lymphocytes have an atypical CD27- memory phenotype and together with CD8+ T cells promote favorable prognosis in ovarian cancer. Clin Cancer Res 18:3281–3292. https://doi.org/10.1158/1078-0432.Ccr-12-0234
4. Wennhold K, Thelen M, Lehmann J et al (2021) CD86(+) antigen-presenting B Cells are increased in cancer, localize in tertiary lymphoid structures, and induce specific T-cell responses. Cancer Immunol Res 9:1098–1108. https://doi.org/10.1158/2326-6066.Cir-20-0949
5. Nielsen JS, Nelson BH (2012) Tumor-infiltrating B cells and T cells: working together to promote patient survival. Oncoimmunology 1:1623–1625. https://doi.org/10.4161/onci.21650
6. Laumont CM, Banville AC, Gilardi M et al (2022) Tumour-infiltrating B cells: immunological mechanisms, clinical impact and therapeutic opportunities. Nat Rev Cancer 22:414–430. https://doi.org/10.1038/s41568-022-00466-1
7. Fridman WH, Sibéril S, Pupier G et al (2023) Activation of B cells in tertiary lymphoid structures in cancer: anti-tumor or anti-self? Semin Immunol 65:101703. https://doi.org/10.1016/j.smim.2022.101703
8. Vivas-García Y, Efeyan A (2022) The metabolic plasticity of B cells. Front Mol Biosci 9:991188. https://doi.org/10.3389/fmolb.2022.991188
9. Noushmehr H, D'Amico E, Farilla L et al (2005) Fatty acid translocase (FAT/CD36) is localized on insulin-containing granules in human pancreatic beta-cells and mediates fatty acid effects on insulin secretion. Diabetes 54:472–481. https://doi.org/10.2337/diabetes.54.2.472
10. Nakamura MT, Yudell BE, Loor JJ (2014) Regulation of energy metabolism by long-chain fatty acids. Prog Lipid Res 53:124–144. https://doi.org/10.1016/j.plipres.2013.12.001
11. Weisel FJ, Mullett SJ, Elsner RA et al (2020) Germinal center B cells selectively oxidize fatty acids for energy while conducting minimal glycolysis. Nat Immunol 21:331–342. https://doi.org/10.1038/s41590-020-0598-4
12. Ramakrishnan R, Tyurin VA, Veglia F et al (2014) Oxidized lipids block antigen cross-presentation by dendritic cells in cancer. J Immunol 192:2920–2931. https://doi.org/10.4049/jimmunol.1302801
13. Nath S, Saad MA, Pigula M et al (2019) Photoimmunotherapy of Ovarian Cancer: a unique niche in the management of advanced disease. Cancers. https://doi.org/10.3390/cancers11121887
14. Schoutrop E, Moyano-Galceran L, Lheureux S et al (2022) Molecular, cellular and systemic aspects of epithelial ovarian cancer and its tumor microenvironment. Semin Cancer Biol 86:207–223. https://doi.org/10.1016/j.semcancer.2022.03.027
15. Almeida-Nunes DL, Mendes-Frias A, Silvestre R et al (2022) Immune tumor microenvironment in Ovarian Cancer ascites. Int J Mol Sci. https://doi.org/10.3390/ijms231810692
16. Wróblewski M, Szewczyk-Golec K, Hołyńska-Iwan I et al (2021) Characteristics of selected adipokines in ascites and blood of Ovarian Cancer patients. Cancers. https://doi.org/10.3390/cancers13184702
17. Luo X, Xu J, Yu J et al (2021) Shaping immune responses in the tumor microenvironment of Ovarian Cancer. Front Immunol 12:692360. https://doi.org/10.3389/fimmu.2021.692360
18. Tian W, Lei N, Zhou J et al (2022) Extracellular vesicles in ovarian cancer chemoresistance, metastasis, and immune evasion. Cell Death Dis 13:64. https://doi.org/10.1038/s41419-022-04510-8
19. Liu B, Nash J, Runowicz C et al (2010) Ovarian cancer immunotherapy: opportunities, progresses and challenges. J Hematol Oncol 3:7. https://doi.org/10.1186/1756-8722-3-7
20. DiSilvestro P, Banerjee S, Colombo N et al (2023) Overall survival with maintenance Olaparib at a 7-year follow-up in patients with newly diagnosed advanced Ovarian Cancer and a BRCA mutation: The SOLO1/GOG 3004 trial. J Clin Oncol 41:609–617. https://doi.org/10.1200/jco.22.01549
21. Zebley CC, Zehn D, Gottschalk S et al (2024) T cell dysfunction and therapeutic intervention in cancer. Nat Immunol 25:1344–1354. https://doi.org/10.1038/s41590-024-01896-9
22. Yu C, Niu X, Du Y et al (2020) IL-17A promotes fatty acid uptake through the IL-17A/IL-17RA/p-STAT3/FABP4 axis to fuel ovarian cancer growth in an adipocyte-rich microenvironment. Cancer Immunol Immunother 69:115–126. https://doi.org/10.1007/s00262-019-02445-2
23. Shin CA, Cho HW, Shin AR et al (2016) Co-expression of CD40L with CD70 or OX40L increases B-cell viability and antitumor efficacy. Oncotarget 7:46173–46186. https://doi.org/10.18632/oncotarget.10068
24. Lee-Chang C, Miska J, Hou D et al (2021) Activation of 4-1BBL+ B cells with CD40 agonism and IFNγ elicits potent immunity against glioblastoma. J Exp Med. https://doi.org/10.1084/jem.20200913
25. Yang X, Li C, Yang H et al (2024) Programmed remodeling of the tumor milieu to enhance NK cell immunotherapy combined with

chemotherapy for pancreatic cancer. Nano Lett 24:3421–3431. https://doi.org/10.1021/acs.nanolett.4c00002
26. Cai D, Li J, Liu D et al (2020) Tumor-expressed B7–H3 mediates the inhibition of antitumor T-cell functions in ovarian cancer insensitive to PD-1 blockade therapy. Cell Mol Immunol 17:227–236. https://doi.org/10.1038/s41423-019-0305-2
27. Sautès-Fridman C, Petitprez F, Calderaro J et al (2019) Tertiary lymphoid structures in the era of cancer immunotherapy. Nat Rev Cancer 19:307–325. https://doi.org/10.1038/s41568-019-0144-6
28. Bao X, Lin X, Xie M et al (2024) Mature tertiary lymphoid structures: important contributors to anti-tumor immune efficacy. Front Immunol 15:1413067. https://doi.org/10.3389/fimmu.2024.1413067
29. Zheng L, Katyal P, Mauldin IS (2025) Methods for analysis of tertiary lymphoid structures and immune activity by multiplex immunofluorescence histology. Methods Cell Biol 199:37–49. https://doi.org/10.1016/bs.mcb.2025.03.008
30. Rossetti RAM, Tordesillas L, Beatty MS et al (2025) CD40L stimulates tumor-infiltrating B-cells and improves ex vivo TIL expansion. J Immunother Cancer. https://doi.org/10.1136/jitc-2024-011066
31. Michalek RD, Gerriets VA, Jacobs SR et al (2011) Cutting edge: distinct glycolytic and lipid oxidative metabolic programs are essential for effector and regulatory CD4+ T cell subsets. J Immunol 186:3299–3303. https://doi.org/10.4049/jimmunol.1003613
32. Waters LR, Ahsan FM, Wolf DM et al (2018) Initial B Cell activation induces metabolic reprogramming and mitochondrial remodeling. iScience 5:99–109. https://doi.org/10.1016/j.isci.2018.07.005
33. Xu S, Chaudhary O, Rodríguez-Morales P et al (2021) Uptake of oxidized lipids by the scavenger receptor CD36 promotes lipid peroxidation and dysfunction in CD8(+) T cells in tumors. Immunity 54:1561–77.e7. https://doi.org/10.1016/j.immuni.2021.05.003
34. Won WJ, Bachmann MF, Kearney JF (2008) CD36 is differentially expressed on B cell subsets during development and in responses to antigen. J Immunol 180:230–237. https://doi.org/10.4049/jimmunol.180.1.230
35. Kobayashi S, Phung HT, Tayama S et al (2021) Fatty acid-binding protein 3 regulates differentiation of IgM-producing plasma cells. Febs j 288:1130–1141. https://doi.org/10.1111/febs.15460
36. De Siqueira MK, Li G, Zhao Y et al (2024) PPARγ-dependent remodeling of translational machinery in adipose progenitors is impaired in obesity. Cell Rep 43:114945. https://doi.org/10.1016/j.celrep.2024.114945
37. Hu J, Li Y, Lian B et al (2025) Mechanism and role of regulated cell death in tumor immunity and immunotherapy. Cancer Commun 45:1456–1495. https://doi.org/10.1002/cac2.70064
38. Guo Z, Liu Y, Chen D et al (2025) Targeting regulated cell death: Apoptosis, necroptosis, pyroptosis, ferroptosis, and cuproptosis in anticancer immunity. J Transl Int Med 13:10–32. https://doi.org/10.1515/jtim-2025-0004
39. Zimmerer JM, Horne PH, Fiessinger LA et al (2012) Cytotoxic effector function of CD4-independent, CD8(+) T cells is mediated by TNF-α/TNFR. Transplantation 94:1103–1110. https://doi.org/10.1097/TP.0b013e318270f3c0
40. Xu J, Guo R, Jia J et al (2021) Activation of Toll-like receptor 2 enhances peripheral and tumor-infiltrating CD8(+) T cell cytotoxicity in patients with gastric cancer. BMC Immunol 22:67. https://doi.org/10.1186/s12865-021-00459-z
41. Schwingshackl L, Hoffmann G (2014) Monounsaturated fatty acids, olive oil and health status: a systematic review and meta-analysis of cohort studies. Lipids Health Dis 13:154. https://doi.org/10.1186/1476-511x-13-154
42. Carrillo C, Cavia MM, Alonso-Torre S (2012) Role of oleic acid in immune system; mechanism of action; a review. Nutr Hosp 27:978–990. https://doi.org/10.3305/nh.2012.27.4.5783
43. Moro-García MA, Mayo JC, Sainz RM et al (2018) Influence of inflammation in the process of T lymphocyte differentiation: proliferative, metabolic, and oxidative changes. Front Immunol 9:339. https://doi.org/10.3389/fimmu.2018.00339
44. Rossetti RAM, Lorenzi NPC, Yokochi K et al (2018) B lymphocytes can be activated to act as antigen presenting cells to promote anti-tumor responses. PLoS ONE 13:e0199034. https://doi.org/10.1371/journal.pone.0199034
45. Oxley KL, Hanson BM, Zani AN et al (2021) Activated B lymphocytes and tumor cell lysate as an effective cellular cancer vaccine. Cancer Immunol Immunother 70:3093–3103. https://doi.org/10.1007/s00262-021-02914-7
46. Bruno TC, Ebner PJ, Moore BL et al (2017) Antigen-presenting intratumoral B cells affect CD4(+) TIL phenotypes in non-small cell lung cancer patients. Cancer Immunol Res 5:898–907. https://doi.org/10.1158/2326-6066.Cir-17-0075
47. Laumont CM, Nelson BH (2023) B cells in the tumor microenvironment: multi-faceted organizers, regulators, and effectors of anti-tumor immunity. Cancer Cell 41:466–489. https://doi.org/10.1016/j.ccell.2023.02.017
48. Kaneno R, Shurin GV, Tourkova IL et al (2009) Chemomodulation of human dendritic cell function by antineoplastic agents in low noncytotoxic concentrations. J Transl Med 7:58. https://doi.org/10.1186/1479-5876-7-58
49. Yu G, Wu Y, Wang W et al (2019) Low-dose decitabine enhances the effect of PD-1 blockade in colorectal cancer with microsatellite stability by re-modulating the tumor microenvironment. Cell Mol Immunol 16:401–409. https://doi.org/10.1038/s41423-018-0026-y
50. Bishnoi S, Kotasek D, Aghmesheh M et al (2024) Dual CTLA-4 and PD-1 checkpoint blockade using CS1002 and CS1003 (nofazinlimab) in patients with advanced solid tumors: a first-in-human, dose-escalation, and dose-expansion study. Cancer 130:1991–2002. https://doi.org/10.1002/cncr.35226
51. Teillaud JL, Houel A, Panouillot M et al (2024) Tertiary lymphoid structures in anticancer immunity. Nat Rev Cancer 24:629–646. https://doi.org/10.1038/s41568-024-00728-0
52. Zhao L, Xi L, Liu Y et al (2025) The impact of tertiary lymphoid structures on tumor prognosis and the immune microenvironment in colorectal cancer. Biomedicines. https://doi.org/10.3390/biomedicines13030539
53. Su X, Kang D, Wang J et al (2025) Tertiary lymphoid structures associated with improved survival and enhanced antitumor immunity in acral melanoma. npj Precis Oncol 9:103. https://doi.org/10.1038/s41698-025-00891-z
54. Fridman WH, Meylan M, Pupier G et al (2023) Tertiary lymphoid structures and B cells: an intratumoral immunity cycle. Immunity 56:2254–2269. https://doi.org/10.1016/j.immuni.2023.08.009